Liu *et al. Energy Mater* 2024;4:400053
DOI: 10.20517/energymater.2023.99

Energy Materials

Article

Open Access

Check for updates

Recent progress in MXenes-based lithium-sulfur batteries

Hui Liu, Shitong Sun, Bo Jin*

Key Laboratory of Automobile Materials, Ministry of Education, and School of Materials Science and Engineering, Jilin University, Changchun 130022, Jilin, China.

***Correspondence to:** Dr. Bo Jin, Key Laboratory of Automobile Materials, Ministry of Education, and School of Materials Science and Engineering, Jilin University, No. 5988, Renmin Street, Changchun 130022, Jilin, China. E-mail: jinbo@jlu.edu.cn

How to cite this article: Liu H, Sun S, Jin B. Recent progress in MXenes-based lithium-sulfur batteries. *Energy Mater* 2024;4:400053. https://dx.doi.org/10.20517/energymater.2023.99

Received: 11 Dec 2023 **First Decision:** 14 Mar 2024 **Revised:** 20 Apr 2024 **Accepted:** 7 May 2024 **Published:** 29 May 2024

Academic Editors: Jinkui Feng, Jiaqi Huang **Copy Editor:** Fangyuan Liu **Production Editor:** Fangyuan Liu

Abstract

Lithium-sulfur batteries (LSBs) are considered as the potent candidates for next-generation energy storage systems due to their high theoretical energy density. However, some inherent problems, including sulfur insulation, shuttle effect caused by lithium polysulfides, and lithium dendrites, hinder their practical application. Various materials have been studied to address the aforementioned issues. A class of two-dimensional inorganic compounds (MXenes), such as transition metal carbides, nitrides, and carbon nitrides, have recently emerged. In this review, we summarize the characteristics and commonly used preparation methods of MXenes and outline the latest development of MXenes and their composites in LSBs. When utilized as sulfur carriers, modified layers of separators, hosts for lithium metal anodes, and electrolyte additives in LSBs, the diversity of structure, excellent conductivity, and high mechanical strength of MXenes and their composites highlight the competitive advantages. This review provides some ideas for the future development of MXenes in LSBs.

Keywords: MXenes, lithium-sulfur batteries, sulfur hosts, functional separators, lithium metal anodes, electrolytes

INTRODUCTION

With the gradual depletion of fossil fuels, it is urgent to accelerate the development and application of novel energy technologies. Traditional lithium-ion batteries (LIBs), with lithium metal oxides ($LiCoO_2$ and $LiNi_xCo_yMn_{1-x-y}O_2$) or lithium iron phosphate ($LiFePO_4$) as cathodes paired with graphite as anodes, have

been widely utilized in portable electronic devices since invention[1-3]. Although LIBs are highly favored, even when fully developed, their energy density using traditional plug-in cathode materials still lags far behind the demand for high-energy-density electric vehicles and portable electronic products[4,5]. Therefore, the traditional LIBs can no longer meet the future progress trend of various devices, prompting continuous exploration of new battery systems surpassing the traditional lithium-ion rechargeable batteries. It is worth noting that metal-sulfur batteries have become the promising next-generation energy storage technologies[6,7]. Lithium-sulfur batteries (LSBs), a new type of battery, comprise active sulfur as the cathode and lithium metal as the anode, which exert multielectron conversion electrochemistry between elemental sulfur and lithium. They have been paid much attention due to superior theoretical specific capacity (1,675 mAh g^{-1}) and energy density (2,500 Wh kg^{-1}) [Figure 1A] and the abundant sulfur element in Earth's crust[3,8,9].

Figure 1B shows the traditional charge/discharge curves of LSBs, in which a sulfur cathode undergoes a redox process of $S_8 + 16Li^+ + 16e^- \leftrightarrow 8Li_2S$. Figure 1B indicates that S_8 undergoes a series of reactions during charging and discharging, forming lithium polysulfides (LiPSs). There are two obvious platforms during discharge, and sulfur chain length gradually shortens. This process transforms from solid (S_8) to liquid (Li_2S_n, $4 \leq n \leq 8$) to solid (Li_2S_2/Li_2S)[10-12]. Usually, the first discharge plateau appears at 2.3 V, indicating that sulfur first transforms into Li_2S_8, which is reduced to Li_2S_6 and then to Li_2S_4. The second discharge plateau at 2.1 V is ascribed to further reduction of Li_2S_4 to insoluble Li_2S_2/Li_2S. Long-chain LiPSs (Li_2S_n) ($4 \leq n \leq 8$) are easily dissolved in liquid electrolyte. Subsequently, due to the conversion reaction between insoluble Li_2S_2 and Li_2S, the reaction kinetics in this stage is slower than in the previous stage[13,14]. During charging, a reverse cycle of the discharge process is embodied. However, in actual operation, the theoretical capacity of LSBs is usually not achievable due to some drawbacks: (i) The poor conductivities of S_8 and its solid-state discharge products (Li_2S_2/Li_2S) lead to slow redox kinetics and low sulfur utilization; (ii) The shuttle effect caused by the dissolution of long-chain soluble LiPSs in the electrolyte results in low Coulombic efficiency and rapid capacity decay; (iii) The huge volume expansion during charging and discharging processes causes the collapse of electrode structure; and (iv) Lithium metal anodes with high chemical activity are prone to participate in side reactions. During charging and discharging, the non-uniform lithium deposition of metal Li forms lithium dendrites[15,16].

Various means have been developed to tackle the aforementioned questions, for example, designing advanced sulfur cathodes, functionalizing separators to physically or chemically constrain LiPSs, and modifying lithium anodes to suppress dendritic growth. Therefore, the design and engineering of various functional materials for LSBs are crucial[17-19]. Porous carbon materials have been widely studied due to their outstanding electronic conductivity, high specific surface area, low cost, and stability. Yet, resulting from low interaction between non-polar porous carbon material and polar LiPS, LiPS slowly transforms on the surfaces, leading to a low utilization rate of active materials. Therefore, the polar materials, including heteroatom-doped materials, various metal compounds, metal-organic frameworks and their derivatives, have become the mainstream in the research of LSBs[3,20]. More recently, MXenes have become competitive candidates among the various functional materials due to their excellent metal conductivity, mechanical strength, rich surface terminals, and strong interaction with LiPSs[21]. They are emerging two-dimensional (2D) materials containing transition metal carbides, nitrides, and carbonitrides. MXenes are prepared by selectively etching "A" layers from MAX ($M_{n+1}AX_n$, n = 1-4) phases, where M equals to transition metal (Sc, Ti, V, Cr, Zr, Nb, Mo), A is typically a IIIA or IVA element, and X represents carbon and/or nitrogen[22-24]. Figure 2A shows various elements used to synthesize MXenes in the periodic table of elements. In addition, all the MXenes can be expressed as ($M_{n+1}X_nT_x$), in which M and X have the same meanings as in $M_{n+1}AX_n$, and T_x corresponds to surface groups (-OH, -O, and/or -F) [Figure 2B][25]. Naguib *et al.* first discovered

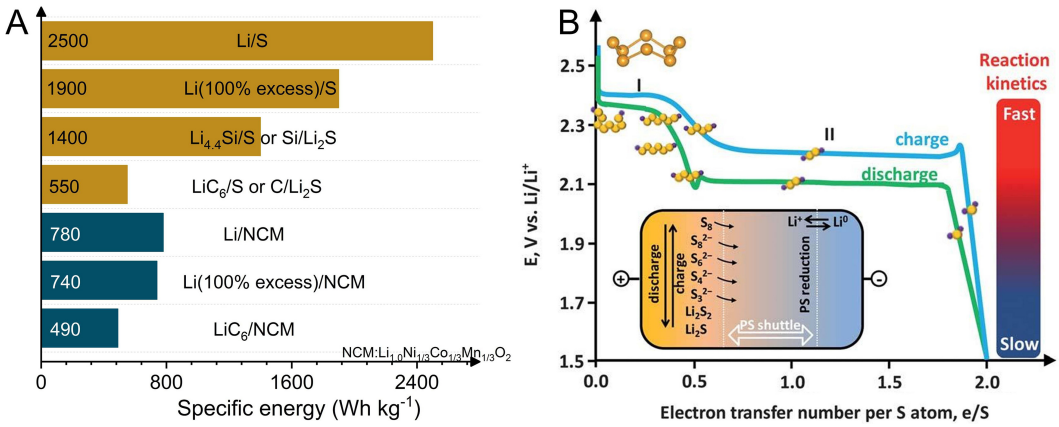

Figure 1. (A) Histograms of specific energies of various rechargeable batteries. Reproduced from Ref.[3] with permission from WILEY-VCH. (B) Typical charge/discharge profiles of LSBs. Reproduced from Ref.[12] with permission from the Royal Society of Chemistry.

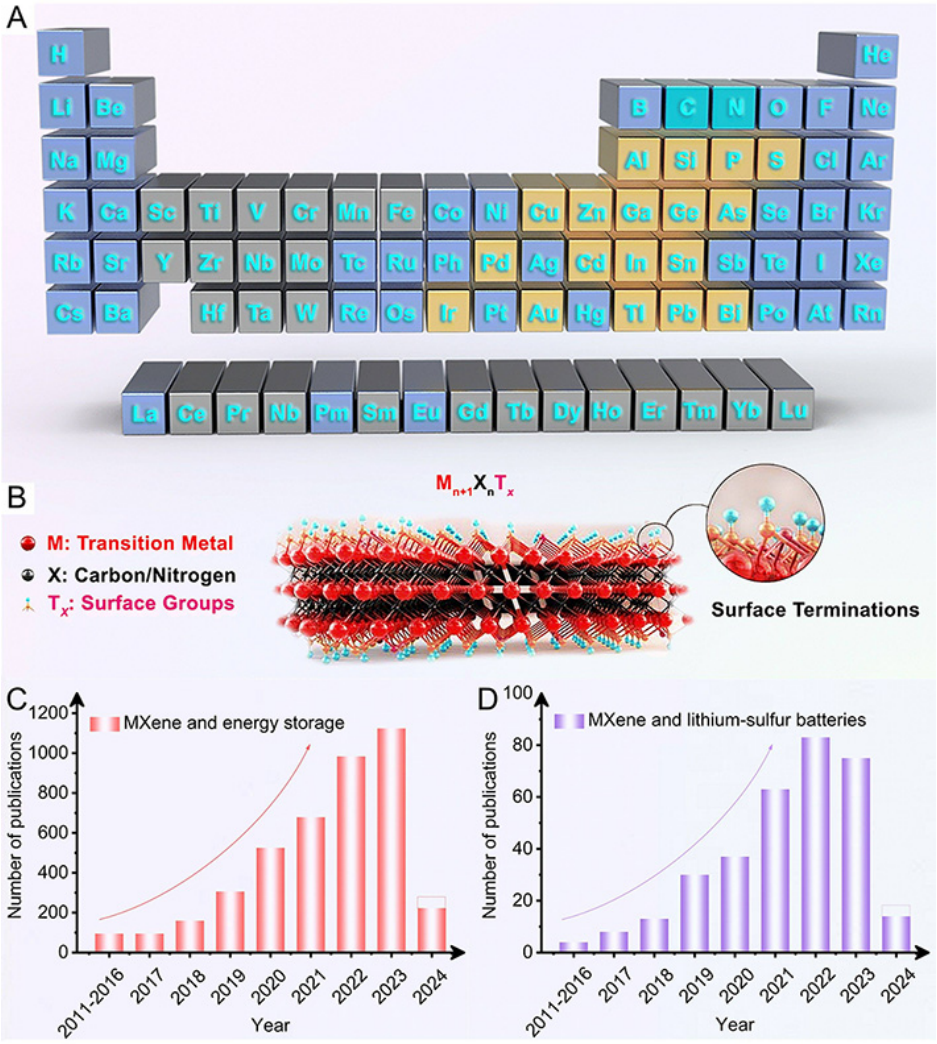

Figure 2. (A) Periodic table of elements including "M", "A", and "X" of MAX. (B) Schematic of MXene structures. Reproduced from Ref.[25] with permission from the Royal Society of Chemistry. Publications about (C) "MXene and energy storage" and (D) "MXene and lithium-sulfur batteries". Data derived from Web of Science.

MXenes in 2011[26]. So far, dozens of them have been prepared and widely used in energy storage [Figure 2C]. At the same time, reports on LSBs based on MXenes are also increasing yearly [Figure 2D].

This review systematically summarizes the research progress of MXenes-based materials in the field of LSBs. Firstly, the basic principle of LSBs is explained, and the characteristics and synthesis methods of MXenes are comprehensively outlined. The application of MXenes-based materials in LSBs is mainly discussed, including MXenes-based materials used for sulfur carriers, modification layers of separators, main hosts of lithium metal anodes, and additives utilized in solid-state electrolytes for LSBs. An intuitive introduction is shown in Figure 3. Finally, the advantages of MXenes and suggestions for future research on MXenes in LSBs are fully summarized and proposed to promote the development of MXenes-based LSBs.

PROPERTIES AND PREPARATION OF MXENES

Properties of MXenes

Structural properties

Since MXenes typically come from their parent MAX, they maintain the unique layered structures of precursors. Meanwhile, their crystal structures are tightly packed hexagonal structures of M atoms, while X atoms fill the gap sites of octahedrons. According to different "M", MXenes are divided into three types: M_2X, M_3X_2, and M_4X_3. M_5C_4 is later produced, further enriching the structural diversity. However, differences exist in the arrangement of M atoms in M_2X compared to M_3X_2 and M_4X_3. In M_2X, these atoms exhibit hexagonal tight stacking (ABABAB), but in M_3C_2 and M_4C_3, they display face-centered cubic stacking (ABCABC)[21,27]. According to previous reports, various preparation methods import different terminals on the surfaces of MXenes, thereby obtaining distinct MXenes. For example, 2D $Ti_2C(OH)_xF_y$ and Ti_2CO_x were received through a series of treatments on Ti_2AlC[28]. In addition, through density functional theory (DFT) calculations, Hu *et al.* found that Ti_3C_2 with terminal modification had a smaller *a* parameter and a larger *d* value (vertical distance between the top and bottom atomic layers) compared to pure Ti_3C_2[29]. After introducing terminal groups, the bond length of Ti1-C located at the center becomes short, while that of Ti2-C in the surface is stretched, proving the strong interaction between the surface terminal and original Ti_3C_2 block. Therefore, when applied to LSBs, MXenes with various terminal functional groups may display strong capture ability for LiPSs and increase chemical and catalytic interaction with sulfur species.

Electronic properties

In addition to the structural properties, MXenes also possess other important properties, with metal conductivity being the most significant. All the MXenes exhibit metallic properties without any surface functionalization[30,31]. However, after surface terminal modification, Sc_2CF_2, $Sc_2C(OH)_2$, Sc_2CO_2, Ti_2CO_2, Zr_2CO_2, and Hf_2CO_2 become semiconductors with a bandgap of approximately 0.25-2.0 eV. Figure 4A presents a direct bandgap for $Sc_2C(OH)_2$, while other semiconductors possess an indirect bandgap, possibly due to Ti, Zr, and Hf having the same numbers of outermost electrons. Therefore, when modifying them with the same functional groups, the corresponding MXenes display similar electronic properties near Fermi energy. Meanwhile, in most MXenes, the p-band of carbon/nitrogen is lower than the d-band of transition metals. It is observed that in all the functionalized MXenes discussed, due to higher electronegativity of X (C and N) atoms and connected functional groups compared to transition metals, transition metals become positively charged by losing electrons[30]. Additionally, the electronic properties of monolayer $Ti_3C_2X_2$ (X = F, Cl, Br, I) functionalized with halogen atoms have also been studied. For the original Ti_3C_2 monolayer, the main contribution to densities of states (DOS) below the Fermi level comes from Ti-C bonds. For $Ti_3C_2X_2$ (X = F, Cl, Br, I), new bands related to Ti-X bonds appear in the energy range between -8 and -2 eV. In summary, a series of calculations indicate that $Ti_3C_2X_2$, functionalized with halogen atoms, maintains its metallic properties[32]. Interestingly, Zhang *et al.* investigated the relationship between the metallic properties and strain of some multilayer MXenes[33]. It was found that V_2CO_2 and

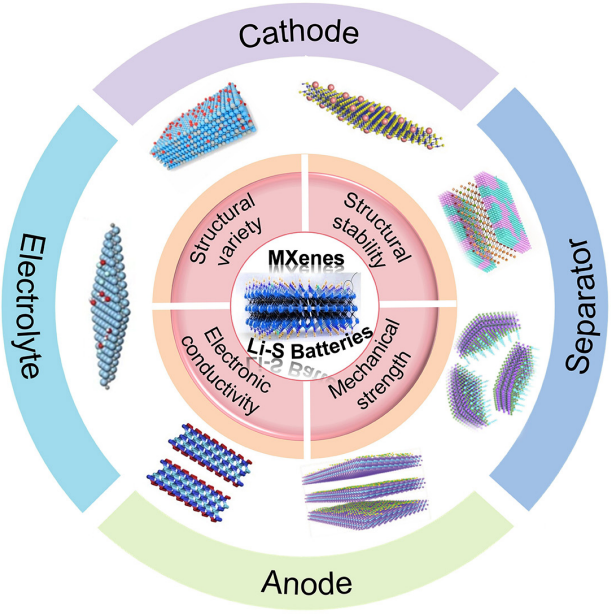

Figure 3. Schematic of application of MXenes-based materials in LSBs.

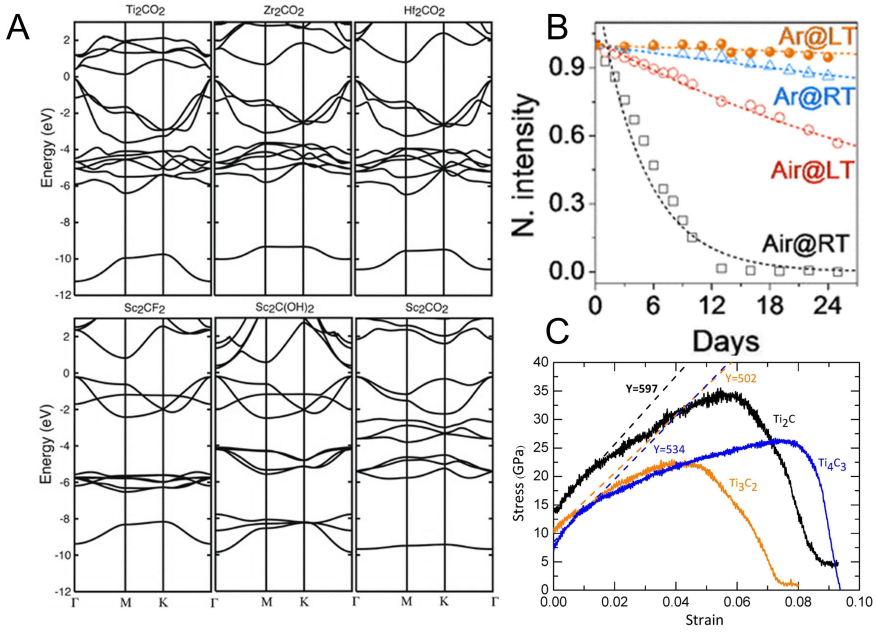

Figure 4. (A) Band structures of semiconducting MXene systems (Fermi energy is located at zero). Reproduced from Ref.[30] with permission from WILEY-VCH. (B) Stability of colloidal d-$Ti_3C_2T_x$ in different environments. The dotted lines are the fitting results according to the empirical equation $A = A_{unre} + A_{re}e^{-t/\tau}$. Reproduced from Ref.[39] with permission from the American Chemical Society. (C) Strain-stress curves obtained by stretching $Ti_{n+1}C_n$ materials. The dashed lines are extrapolated from the initial linear regions of strain-stress curves. Reproduced from Ref.[44] with permission from IOP Publishing.

Nb_2CO_2 materials showed metallic properties at the initial stage, while their metallic properties were maintained with the strain variation. However, with increasing compressive strain, the multilayer Hf_2CO_2 and Zr_2CO_2 materials significantly transition from semiconductors to metal. In addition, the experiments have demonstrated that the synthesis conditions significantly influence the electronic properties of $Ti_3C_2T_x$. Lipatov *et al.* reported an improved synthesis method for preparing high-quality monolayer $Ti_3C_2T_x$

flakes[34]. The $Ti_3C_2T_x$ flakes exhibited a high conductivity of 4,600 ± 1,100 S cm^{-1}. An "evaporated-nitrogen" minimally intensive layer delamination (EN-MILD) approach was used to obtain high-quality MXene sheets. Through this method, the conductivity of $Ti_3C_2T_x$ MXenes increased up to 2.4 × 10^4 S cm^{-1}[35]. Moreover, because of their high strength and metal conductivity, 2D $Ti_3C_2T_x$ flakes were commonly utilized to prepare the conductive films. A scalable approach prepared strong and highly conductive pure MXene films with highly arranged large MXene flakes. It was found that a film with a thickness of 214 nm possessed a conductivity of approximately 15,100 S cm^{-1}[36].

Structural stability

The stability of MXenes is also a key parameter that affects their application. According to the above discussion, their diverse terminals will affect their properties and stability. Therefore, Xue *et al.* explored how different terminals affect stability of Ti_2C[37]. It was found that F-Ti_2C solution underwent complete oxidation within 36 h, and this could not be changed even at 4 °C. As the proportion of F in the terminal group increased, that of low oxidation state Ti also augmented, leading to the instability of F-terminal MXenes. In contrast, O-Ti_2C stored well at room temperature. The stability of O-Ti_2C was much better than that of F-Ti_2C, mainly due to the contribution of abundant O terminal groups. Moreover, many previous studies have shown that water is not the optimal medium for storing as-synthesized $Ti_3C_2T_x$. $Ti_3C_2T_x$ formed TiO_2 under certain conditions[38]. Zhang *et al.* tested the stability of MXene aqueous solutions under different conditions (air at low temperature (Air@LT), argon at room temperature (Ar@RT), argon at low temperature (Ar@LT), and air at room temperature (Air@RT)), indicating that the best result was achieved under the condition of Ar@LT [Figure 4B][39]. Compared with air atmosphere, the stability of samples stored under Ar had been significantly improved. Meanwhile, the low-temperature environment also made an important contribution to the stability of d-$Ti_3C_2T_x$ aqueous solutions. Researchers found that when stored at -80 °C, the aqueous solutions of $Ti_3C_2T_x$ MXene maintained chemical stability for more than 39 weeks. When the dispersion medium was replaced with ethanol, even at 5 °C, the degradation process was procrastinated[40]. Furthermore, introducing antioxidants (ascorbic acid) also enhanced the oxidative stability of MXenes. Meanwhile, it was proven that MXenes with higher "n" possessed stronger oxidation stability[41]. Moreover, the stability of MXene thin films has also been studied. Lee *et al.* reported the hydrogen annealing strategy for enhancing oxidation stability of Ti_3C_2 MXene films[42]. The outcomes implied that sheet resistance of oxidized Ti_3C_2 MXene film could be restored through hydrogen annealing, and the oxidation stability was significantly improved under the severe conditions (100% relative humidity, 70 °C). This research promoted the applications of MXene films in the harsh conditions such as open air, high temperature, and high humidity.

Mechanical properties

MXenes themselves possess satisfactory mechanical stability, allowing them to buffer volume expansion of sulfur when used as sulfur carriers in LSBs[43]. Borysiuk *et al.* explored mechanical characteristics of 2D titanium carbides using classical molecular dynamics methods[44]. The obtained stress-strain plots during the tensile deformation process of titanium carbides are shown in Figure 4C. The thinnest Ti_2C had the highest Young's modulus compared to T_3C_2 and T_4C_3. And under critical stress, all the $Ti_{n+1}C_n$ samples displayed similar behavior. In addition, for currently considered MXenes, the surface functionalization enhanced the mechanical properties by decreasing Young's modulus and prolonging the critical strain[45]. Chen *et al.* investigated the influence of MXenes [$Ti_3C_2O_2$ and $Ti_3C_2(OH)_2$] with different terminals on the mechanical properties[46]. The calculation results indicated that $Ti_3C_2O_2$ with -O terminal possessed higher strength than $Ti_3C_2(OH)_2$ with -OH terminal. Moreover, adding MXenes also improved the mechanical properties of polymers. The tensile strength of polyvinyl alcohol (PVA)-MXene2 obviously increased due to the interface interaction between MXene and PVA matrix compared to pure PVA films. The hydrogen bond, probably

generated between -OH groups between the MXene layer and PVA, boosted the mechanical properties by forming a rigid network[47]. The large number of spaces in the MXene films reduced their mechanical properties. Wan *et al.* effectively removed voids by adopting the sequential bridging of hydrogen and covalent bonding agents, thus obtaining very dense MXene films[48]. As hydrogen and covalent bonding agents can induce densification and enhance interlayer interaction, the mechanical properties of hydrogen-bonded MXene (HBM) and covalently bridged MXene (CBM) were improved. Due to the synergistic densification brought out by hydrogen and covalent bonding agents, the sequentially bridged MXene (SBM) films possessed the outstanding tensile strength (583 ± 16 MPa) and Young's modulus (27.8 ± 2.8 GPa).

Preparation of MXenes

HF etching approach

Since the emergence of MXenes, HF etching has been identified as the simplest method for preparing different MXenes[26,49]. Naguib *et al.* first obtained 2D Ti_3C_2 nanosheets by exfoliating Ti_3AlC_2 in HF[26]. The exposed Ti surface was capped by OH and/or F. Therefore, when Ti_3AlC_2 is immersed in HF, the following simplified reactions occur:

$$Ti_3AlC_2 + 3HF = AlF_3 + 3/2H_2 + Ti_3C_2 \quad (1)$$

$$Ti_3C_2 + 2H_2O = Ti_3C_2(OH)_2 + H_2 \quad (2)$$

$$Ti_3C_2 + 2HF = Ti_3C_2F_2 + H_2 \quad (3)$$

DFT optimization results indicate that the stripped 2D Ti_3C_2 layer contains two exposed Ti atoms per unit of molecular formula, and the suitable ligands are needed to fill it. Due to fluoride ions and aqueous solution in the preparation environment, hydroxyl and fluorine are the most probable ligands. Compared with -OH, due to higher electronegativity of F, the charge transfer for F between Ti atoms of MXene and the terminal group will be large, making F-Ti bonds stronger than Ti-OH bonds. F-terminal provides higher structure stability[50]. To enhance the delamination of MXene nanosheets, it is usually necessary to increase interlayer spacing and degrade interaction between adjacent layers. Various intermediates, including dimethyl sulfoxide, N, N-dimethylformamide, and tetrapropylammonium hydroxide, have been introduced[51-53]. The effects of time and temperature on the synthesis process of MXenes were also investigated. Etching at 60 °C in 49% HF solution required at least 24 h. In an oxygen atmosphere, some MXene layers were oxidized at 200 °C, while MXenes were completely oxidized at 1,000 °C[54]. Nevertheless, Ti_3C_2 MXene remained intact at 1,200 °C under Ar. In addition, -OH and -F groups attached to the surface of Ti_3C_2 nanosheets are eliminated through heat treatment. At the same time, the nanoscale defects are also cleared off using this method, maintaining hexagonal crystal structure of MXene[55].

F-based salt etching approach

Using hydrofluoric acid to prepare MXenes is the most classic and efficient strategy, but the concentrated hydrofluoric acid used in the procedure is very dangerous. On this basis, a new method has been discovered and widely adopted, replacing hydrofluoric acid with lithium fluoride and hydrochloric acid[56-58]. Ghidiu *et al.* obtained high-yield MXene using LiF and HCl[56]. This technique did not cause material losses, and the yield of MXene after etching was approximately 100%, comparable with HF etching methods. MXene thin film received using LiF and HCl possessed a larger lateral size and a milder etching environment than HF etchant. Ebrahimi *et al.* synthesized $Ti_3C_2T_x$ MXene by LiF/HCl solution[57]. As the etchant concentration increased, the Al etching became more effective, resulting in the typical $Ti_3C_2T_x$ MXene layered structure. Using HF as an etchant results in more defects on MXene flakes, while LiF/HCl

etchant does not exhibit this phenomenon[49]. Inspired by hydrochloric acid and lithium fluoride, other fluoride salts mixed with HCl are also used to synthesize MXenes to varying degrees, and these etchants exhibit similar etching behavior[59-61]. During the synthesis of V_2C MXene, Wu *et al.* investigated the effects of three different etching solutions: LiF + HCl, NaF + HCl, and KF + HCl[59]. The difference among them is the kind of cation. However, in etching aqueous solutions, the cations are hydrated. The radius of $[Na(H_2O)_y]^+$ is greater than that of $[K(H_2O)_z]^+$, and the concentration is much higher than that of $[Li(H_2O)_x]^+$. Therefore, NaF + HCl is the optimal choice for synthesizing V_2C MXene.

Molten salt etching approach

Anyway, the above two methods inevitably use strong acids, which not only pollute the environment but also cause many risks in the synthesis processes. Recently, a molten salt (MS) etching method has provided a new channel for preparing MXenes. Urbankowski *et al.* first utilized molten fluoride salts and Ti_4AlN_3 precursors to synthesize 2D titanium nitride $Ti_4N_3T_x$ (T = F, O, OH) in an Ar atmosphere at 550 °C[62]. DFT results of $Ti_4N_3T_x$ demonstrated that the O terminal on $Ti_4N_3T_x$ (T = O) was the most energetically advantageous compared with F and OH. Therefore, MXenes with different terminals were prepared by selecting MSs[63,64]. Khan *et al.* synthesized Ti_3C_2 MXene by etching MAX phase based on direct redox coupling between element A and cation of Lewis acid MS. Specifically, Ti_3AlC_2, NaCl, KCl, and MSs ($CuCl_2$, $CuBr_2$, CuI_2) were uniformly mixed at different ratios and then annealed in an Ar atmosphere[63]. After reaction, Ti_3C_2 MXenes with halogen terminals were obtained. Lewis-acid-melt etching can finely control the surface structure of MXenes, which can also prepare other materials in the MXenes family.

Alkali-assisted etching approach

In recent years, some methods that use alkali-assisted etching have also been reported due to the special properties of aluminum, and Al can react with both acid and base[65, 66]. Xuan *et al.* obtained 2D functionalized titanium carbide using an organic base (tetramethylammonium hydroxide, TMAOH) as an etchant to etch Ti_3AlC_2 [65]. The reason for choosing TMAOH might be because it was very useful for Al etching, and the cleavage of the Ti-Al bond allowed the bulky tetramethylammonium cation (TMA^+) to enter the channel space, thus promoting the stratification of titanium carbide. In addition, Li *et al.* first prepared a MXene ($Ti_3C_2T_x$, T = OH, O) only using alkaline etching[66]. The results indicated that the multi-layer $Ti_3C_2T_x$ (m-$Ti_3C_2T_x$) with OH and O terminals and a purity of approximately 92 wt% were obtained under 27.5 M NaOH and 270 °C. The entire preparation process contained no fluorine. The as-obtained $Ti_3C_2T_x$ membrane electrode exhibited satisfactory capacitive performance in 1 M H_2SO_4.

Other approaches

Some other synthesis routes have gradually been explored, such as electrochemical etching[67,68], chemical vapor deposition (CVD)[69], iodine (halogen)-assisted etching[70],*etc.* Chen *et al.* proposed a simple electrochemical etching strategy[67]. F-free and Cl-containing $Ti_3C_2T_x$ with plurinatality was prepared under the mixed aqueous solution condition of lithium hydroxide and chloride. In addition, the introduction of Li^+ in electrolyte (0.8 M LiOH and 1.0 M LiCl) enabled it to be embedded in the $Ti_3C_2T_x$ layer, and reduced the interaction between layers, which was beneficial for layering of m-$Ti_3C_2T_x$, effectively avoiding superposition once again. Therefore, after ultrasonic treatment, $Ti_3C_2T_x$ thin film with a transverse size of ~3.8 μm and a thickness of ~3.9 nm was obtained. Wang *et al.* adopted the CVD method to demonstrate a direct synthesis route for scalable and economic synthesis of MXenes, achieving excellent lithium-ion storage performance[69]. Shi *et al.* indicated a fluorine-free and iodine-assisted etching method to acquire 2D MXenes ($Ti_3C_2T_x$, T = O, OH)[70]. The obtained MXene sheets had a yield of up to 71%, a large size of 1.8 μm, and a final thickness of less than 5 nm. The as-prepared film possessed excellent conductivity and stability in aqueous media. This provides an important research value for simple and sustainable production of highly stable MXenes in the future.

In conclusion, MXenes are synthesized using different methods. Each preparation embodies the diverse advantages and disadvantages, as seen in Table 1 for details.

DEVELOPMENT OF MXENES IN LSBS

LSBs have been widely studied in secondary battery systems because of their high energy density. However, some serious issues, including poor conductivities of active sulfur and dissolution of discharge products, hinder their further commercial application[15,16]. Therefore, seeking various materials for high-performance LSBs has become a research hotspot. As is well known, graphene, one of 2D materials, has been a promising material for LSBs because of its outstanding conductivity and chemical stability[71]. However, because it only contains a carbon skeleton, its low polarity and simple chemical composition result in poor anchoring for LiPSs and slow reaction kinetics. Moreover, the lack of diverse functional groups on the graphene surface hinders its further development[72]. However, MXenes have the accordion-like structure more favorable for storing sulfur atoms than graphene[73]. They also possess excellent conductivities and high specific surface areas[55]. Therefore, when applied in LSBs, their large specific surface areas provide sufficient spaces to contact with sulfur. And they also supply satisfactory electron transfer sites for active sulfur. In addition, the interlayer space effectively eases volume expansion during charging and discharging[74]. Previous reports have found that the "acid" Ti sites and hydroxy terminal groups strongly interact with LiPSs and have intense chemical adsorption for LiPSs[75]. At the same time, by assembling 2D MXene nanosheets into a porous connected 3D network structure, a larger space accommodates lithium and reduces local current density, effectively regulating Li plating behavior[76].

Development of MXenes in cathodes

MXenes have layered graphene-like structure and high conductivity, demonstrating satisfactory electrochemical performance as sulfur hosts of LSBs. As shown in Figure 5A, Tang *et al.* obtained $Ti_3C_2T_x$ by etching Ti_3AlC_2 MAX phase using modified LiF-HCl[77]. This method had a high LiF to MAX molar ratio, allowing all excess Li^+ to migrate into the as-prepared m-$Ti_3C_2T_x$. $Ti_3C_2T_x$/S paper was prepared using a physical vapor deposition technique. A certain proportion of $Ti_3C_2T_x$ paper and sulfur powder were placed in both ends of a quartz tube furnace, heated at 300 °C for 5 h under Ar, and followed by heating at 115 °C for 2 h to obtain $Ti_3C_2T_x$/S. The loading capacity of sulfur was 30%. A scanning electron microscopy (SEM) image of $Ti_3C_2T_x$/S is shown in Figure 5B. This sturdy paper inherited the outstanding conductivity and mechanical properties of $Ti_3C_2T_x$ nanosheets. During charging and discharging, a thick sulfate protective layer was formed *in situ* on the $Ti_3C_2T_x$ surface, effectively inhibiting the shuttle of LiPSs and enhancing the utilization rate of sulfur. Therefore, after 1,500 cycles, a satisfactory (0.014%) capacity decay rate was achieved. Due to the involvement of dangerous HF in the synthesis process, Yang *et al.* synthesized MS-$Ti_3C_2T_x$ using $ZnCl_2$ as the MS and Ti_3AlC_2 as the precursor through Lewis etching instead of an F-based salt etching method. Finally, after optimal calcination at 600 °C, layered MS-$Ti_3C_2T_x$-600 [Figure 5C] was obtained[78]. The results indicated that the etching temperature seriously affected the structure and morphology of MS-$Ti_3C_2T_x$, resulting in different electrochemical properties. MS-$Ti_3C_2T_x$/S composite was obtained by mixing MS-$Ti_3C_2T_x$ powder and sulfur in a mass ratio of 3:7 and then heating the mixture at 155 °C through 12 h in Ar. The loading capacity of sulfur was 69.8%. After testing, MS-$Ti_3C_2T_x$-600/S cathodes achieved a first discharge capacity of 987 mAh g^{-1} at 0.1 C [Figure 5D]. Currently, the most common method for synthesizing MXenes is using fluorinated acidic aqueous solutions to etch their MAX phase. Nevertheless, it is not safe and friendly. To this end, a low-temperature "soft chemistry" method according to the photo-Fenton (P.F.) reaction was utilized instead of the etching method to obtain high-purity (95%) fluorine-free Ti_3C_2 (Ff-Ti_3C_2) [Figure 5E and F][79]. Ff-Ti_3C_2/S composite was obtained through

Table 1. Advantages and disadvantages of each preparation method

Synthetic method	Etchant	Advantage	Disadvantage
HF etching approach	HF	Low concentration and short time	Operational hazards
F-based salt etching approach	LiF/NaF/KF + HCl	Mild conditions, Larger flakes and lower defects	Possible residual unetched particles
Molten salt etching approach	LiF + NaF + KF	Synthesis of nitride MXene	High-temperature conditions
Lewis acid molten salt etching approach	Lewis acid	Directional preparation of materials with single surface functional groups	High-temperature conditions
Alkali-assisted etching approach	TMAOH	Expanded layer space, Fluorine-free functional groups	Need to preprocess in HF, Do not shake violently
	NaOH	Fluorine-free functional groups	Severe experimental conditions
Electrochemical etching approach	HCl	Facile and time-saving	Formation of CDC layers
Chemical vapor deposition approach		High quality	High-temperature conditions
Iodine assisted etching method	Iodine	Targeted regulation of surface functional groups	Strict experimental conditions

in-situ deposition of sulfur species on the surface of delaminated Ff-Ti_3C_2. Ff-Ti_3C_2 and $Na_2S_2O_3$ were added into the deionized water. After the alternating ultrasound, the diluted hydrochloric acid was introduced into the above solution, and the reaction lasted for 2 h at N_2. Finally, a flexible self-supporting Ff-Ti_3C_2/S membrane with a sulfur content of ~69.6 wt% was achieved. Experiments demonstrated that LSBs with Ff-Ti_3C_2 cathode had improved rate performance and cycling performance compared to F-terminal Ti_3C_2 (F-Ti_3C_2) cathode. This might be attributed to high mechanical strength and enhanced catalytic conversion ability of Ff-Ti_3C_2 sulfur host for LiPSs. More importantly, when the areal sulfur loading increased to 6.4 mg cm^{-2}, Ff-Ti_3C_2/S electrodes delivered a high capacity of 6.2 mAh cm^{-2} at 0.2 C [Figure 5G].

It is worth noting that although MXenes acquire good performance as sulfur hosts of LSBs because of the strong van der Waals force, MXene nanosheets are restacked, which limits the approachability of ions and reduces the utilization rate of functional surfaces[80]. Therefore, it is necessary to composite MXenes with carbon materials to avoid such accumulation[81-83]. Liang *et al.* prepared a porous conductive network interwoven with MXene nanosheets and carbon nanotubes (CNTs)[84]. Introducing CNTs enhanced the specific surface area and prevented stacking of layered MXene nanosheets [Figure 6A]. S/CNT-MXene composite was acquired through the traditional melt-diffusion method. CNT-MXene was mixed with sulfur in a certain proportion and annealed at 155 °C for 12 h. When the interwoven MXene nanosheet/CNTs composite was applied to a sulfur host of LSBs, due to its strong anchoring ability for LiPSs, LSBs presented excellent long-term cycling stability. Lv *et al.* reported Mo_2C-CNT used as a sulfur host. Firstly, the Mo_2C-CNT and sublimated sulfur (1:8, wt/wt) were mixed evenly[85]. Then, the mixture was annealed at 155 °C for 18 h under Ar to obtain Mo_2C-CNT/S composite. The weight loading of sulfur in Mo_2C-CNT/S is 87.1%. As shown in Figure 6B, hydroxyl-functionalized Mo_2C-based MXene nanosheets were easily prepared by removing Sn layers of Mo_2SnC. By further importing CNTs into the Mo_2C phase, the composite material possessed increased specific surface area, improved electronic conductivity, and accelerated electron transport. In addition, strong chemical adsorption between Mo atoms on surfaces of MXenes and LiPSs effectively restrained the shuttle of LiPSs, thus getting excellent electrochemical performance of LSBs (~925 mAh g^{-1} after 250 cycles at 0.1 C). Other carbon materials are also widely used for compounding with MXenes[86,87].

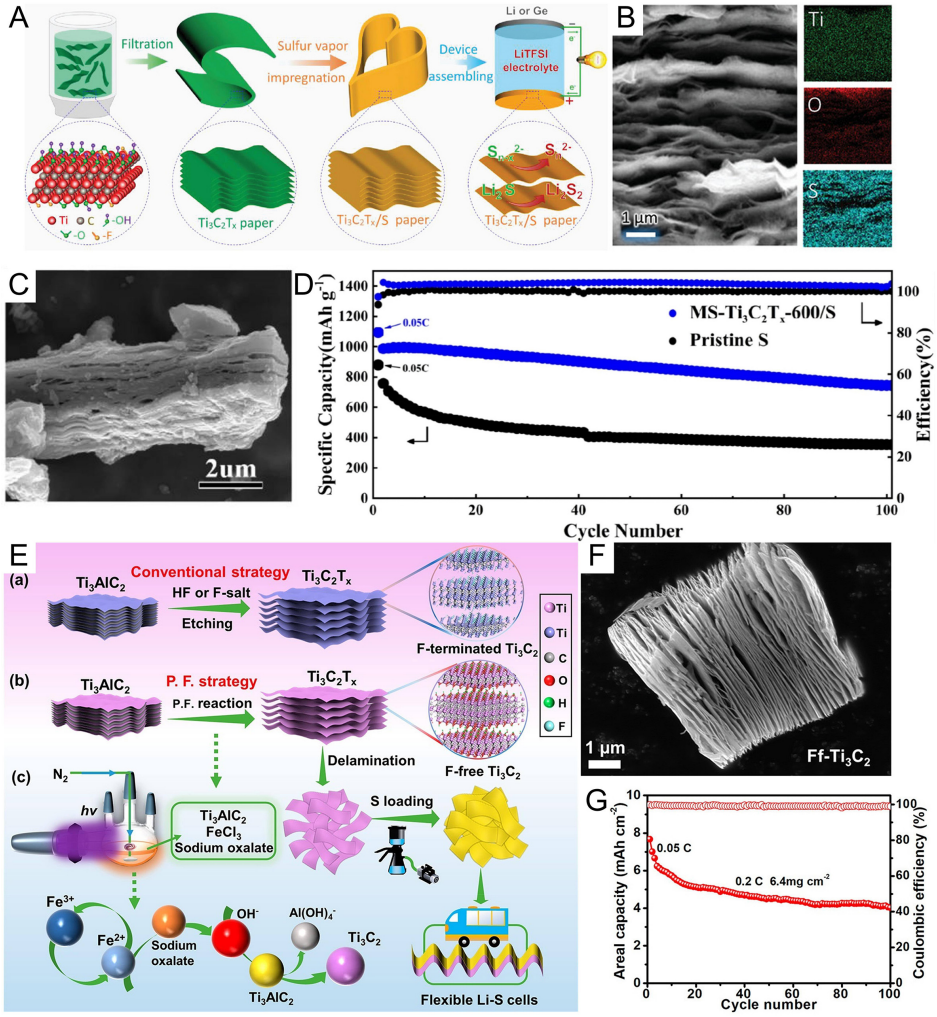

Figure 5. (A) Preparation schematic of robust, freestanding, and conductive $Ti_3C_2T_x$/S paper. (B) Cross-section SEM image of $Ti_3C_2T_x$/S paper and corresponding EDX elemental mappings of Ti, O, and S. Reproduced from Ref.[77] with permission from WILEY-VCH. (C) SEM image of MS-$Ti_3C_2T_x$-600. (D) Cycling performance and the corresponding Coulombic efficiency of MS-$Ti_3C_2T_x$-600/S and the pristine sulfur cathode at 0.1 C. Reproduced from Ref.[78] with permission from Springer. (E) Schematic illustration for the fabrication of F-Ti_3C_2 via a conventional F-containing strategy (a), P.F. strategy for the fabrication of Ff-Ti_3C_2 and its application in flexible Li-S batteries (b), and Fe(III)-oxalato P.F. reaction system (c). (F) SEM image of Ff-Ti_3C_2. (G) Cycling performance of Ff-Ti_3C_2/S with a sulfur loading of 6.4 mg cm^{-2} at 0.2 C. Reproduced from Ref.[79] with permission from the American Chemical Society.

The composites with conductive carbon materials effectively improve the conductivity of composite sulfur cathodes. However, a weak affinity between non-polar carbon and LiPSs leads to poor capacity retention of LSBs during cycling[16]. To improve the affinity for LiPSs, the materials with polar sites, by doping with heteroatoms (N, S, Zn, *etc.*) and metal compounds, were combined with MXenes as sulfur hosts to enhance the capture of LiPSs and accelerate redox kinetics of LiPSs[88-92]. Doping with heteroatoms could regulate the coordination environment and electronic structure of materials, thereby enhancing the electronic conductivity. The doping of heteroatoms could import the additional anionic vacancies and generate a d-band center close to the Fermi level, improving the adsorption and conversion kinetics of LiPSs[93]. As shown in Figure 6C, porous N-doped Ti_3C_2 MXene (P-NTC) as a sulfur host was designed and synthesized using a melamine formaldehyde template route, which not only possessed the porous network [Figure 6D] and excellent conductivity but also strong chemical anchoring and catalytic conversion capabilities for LiPSs. Specifically, P-NTC and sublimated sulfur were uniformly ground in a mass ratio of 1:4. Then, the

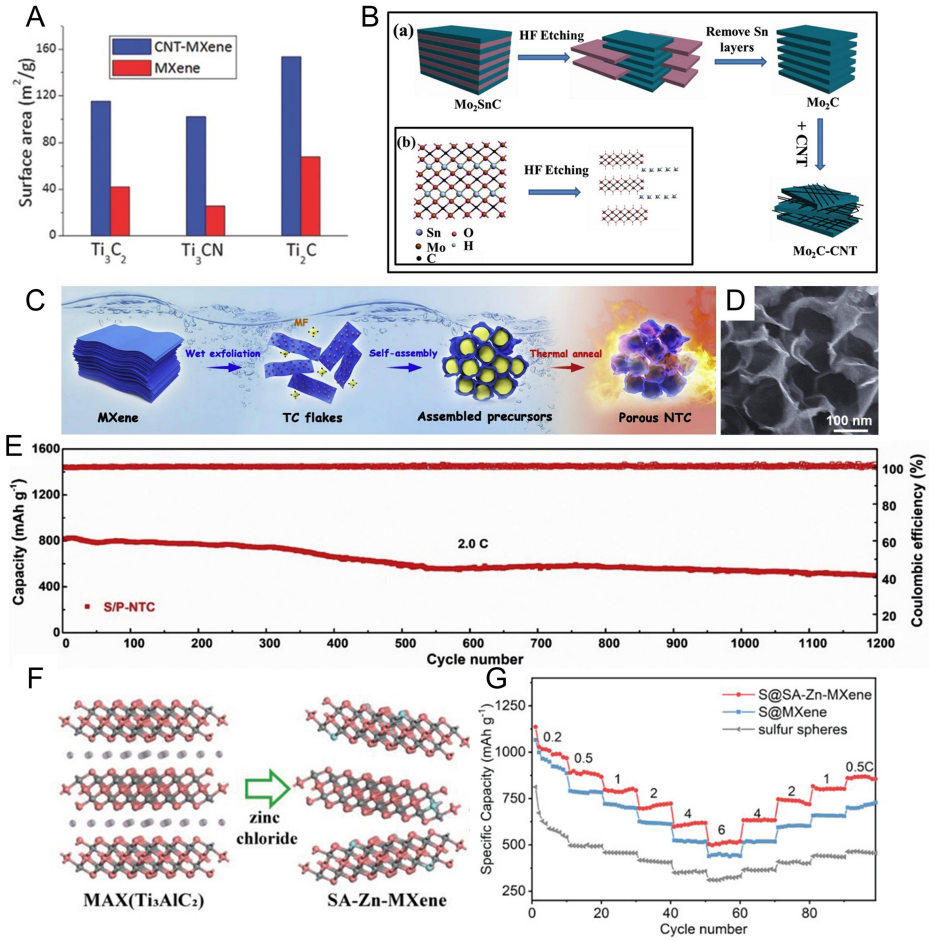

Figure 6. (A) Histograms of surface areas of delaminated MXene nanosheets and CNT-MXene composites. Reproduced from Ref.[84] with permission from WILEY-VCH. (B) Illustrations of synthesis processes of (a) Mo_2C-CNT and (b) Mo_2C. Reproduced from Ref.[85] with permission from WILEY-VCH. (C) Schematic diagram of synthesis of P-NTC. (D) SEM image of P-NTC. (E) Long-term cycling performance of S/P-NTC at 2 C. Reproduced from Ref.[89] with permission from Elsevier. (F) Synthesis diagram of single atom zinc injection into MXene (SA-Zn-MXene). (G) Rate performance of S@SA-Zn-MXene, S@MXene, and sulfur spheres at different current densities. Reproduced from Ref.[92] with permission from WILEY-VCH.

mixture was transferred to a sealed glass container and kept for 6 h at 155 °C to obtain S/P-NTC composite. The sulfur content in the whole cathode was 64%. As expected, the as-obtained S/P-NTC cathode displayed a low capacity decay rate (0.033% per cycle, over 1,200 cycles) at 2.0 C [Figure 6E][89]. The Al layer of Ti_3AlC_2 was etched off using a molten zinc chloride method (600 °C), and the single atom (SA)-Zn-MXene layer was obtained through ultrasonic treatment in Ar-saturated isopropanol [Figure 6F]. Its lateral size was approximately several hundred nanometers. Preparing S@SA-Zn-MXene involved two steps. Firstly, a sulfur sphere suspension was prepared using sodium thiosulfate pentahydrate and polyvinylpyrrolidone. Next, SA-Zn-MXene aqueous dispersion was added into the above solution. Finally, S@SA-Zn-MXene with a sulfur content of 89 wt% was acquired through filtration and freeze-drying treatment. S@SA-Zn-MXene not only had superior affinity for LiPSs, but also played a key role in reducing the conversion energy barrier of Li_2S_2 to Li_2S, which expedited the redox process of LiPSs. In addition, the uniformly distributed zinc atoms in the SA-Zn-MXene layer could also accelerate the nucleation of L_2S_2/Li_2S on MXene layers. Therefore, the S@SA-Zn-MXene obtained a reversible capacity of 1,136 mAh g^{-1} at 0.2 C and outstanding rate capability (517 mAh g^{-1} at 6 C) [Figure 6G][92].

Additionally, polar materials, such as metal sulfides, nitrides, and oxides, have also been compounded with MXenes as sulfur hosts[74,94-100]. Specifically, Tian *et al.* grew VS_4 nanoparticles on the surfaces of MXene nanosheets by the hydrothermal method, and imported graphene oxide (GO) to build a 3D conductive network aerogel [Figure 7A][95]. As shown in Figure 7B-D, there were large-scale pores among the internal sheet-like structures. The GO played a crucial role in bridging various components. The introduction of VS_4 with a straight chain crystal structure enhanced anchoring and catalytic conversion of LiPSs. In addition, the composite between MXene and VS_4 not only stabilized the structure of transition metal sulfide but also accelerated electron migration and improved the adsorption and reversible conversion of LiPSs. Due to these synergistic effects, the as-prepared GO@MXene@VS_4 aerogel effectively inhibited the shuttle effect and enhanced the cycle stability of LSBs. The construction of S/GO@MXene@VS_4 went through the following steps. Firstly, sulfur powder was dissolved in carbon disulfide, and then solution was dropped onto GO@MXene@VS_4 aerogel. Finally, the aerogel with sulfur powder was transferred to a Teflon container filled with Ar and heated at 155 °C for 12 h. The sulfur content in the whole cathode was 58%. The batteries equipped with S/GO@MXene@VS_4 obtained an ultra-low decay rate of 0.019% per cycle after 1,200 cycles at 5 C [Figure 7E]. The heterogeneous Nb_2C/Nb_2O_5 composite material was synthesized for the first time through water-steam etching. Nb_2C nanosheets with high conductivity provided the carrier for formation of Nb_2O_5. The preparation of S-Nb_2C/Nb_2O_5 was as follows: (1) S/CS_2 (0.5 M) solution was slowly dropped into an agate mortar containing Nb_2C/Nb_2O_5 powder and ground evenly; (2) The as-prepared mixture was transferred to a Teflon reactor with Ar and heated at 155 °C for 12 h. The sulfur content of S-Nb_2C/Nb_2O_5 is close to 75 wt%. S-Nb_2C/Nb_2O_5 combined the strong anchoring of Nb_2C with the strong catalytic activity of Nb_2O_5 to achieve rapid capture and conversion of LiPSs. Thanks to synergistic effect of Nb_2C and Nb_2O_5, LSB with S-Nb_2C/Nb_2O_5 positive electrode exhibited excellent electrochemical performance (an area specific capacity of 3.5 mAh cm^{-2} under sulfur loading of 5.3 mg cm^{-2})[96]. For the first time, Zhang *et al.* synthesized oxygen-vacancy-rich Ti_nO_{2n-1} quantum dots (OV-T_nQDs) decorated on porous carbon nanosheets (PCN) (OV-T_nQDs@PCN) nanohybrids using $Ti_3C_2T_x$ as a precursor[97]. OV-T_nQDs@PCN/S with a high S content of 79.1% was obtained by mixing evenly OV-TnQDs@PCN powder with elemental sulfur powder in a mass ratio of 1/4, heating them at 155 °C for 24 h, and then annealing the mixture at 200 °C for 2 h to remove the additional sulfur. Due to synergistic effect of each component, OV-T_nQDs@PCN possessed strong anchoring and catalytic conversion kinetics for LiPSs. Therefore, OV-T_nQDs@PCN/S displayed good rate performance (672 mA h g^{-1} at 2 C), long cycle stability (88% capacity retention rate over 1,000 cycles at 2 C), and sulfur mass loading of 2.2 mg cm^{-2}, demonstrating the application value and potential in high-performance LSBs.

The hollow spheres (HSs) were composed of ultra-thin 2D $Ti_3C_2T_x$-TiN heterostructures (MXene-TiN) and synthesized using melamine-formaldehyde resin (MF) spheres as templates and *in-situ* nitriding by controlling synthesized atmosphere [Figure 8A]. Figure 8B shows a nearly hollow spherical structure of MF@MXene. The surface of MXene was *in-situ* nitrided, forming heterogeneous $Ti_3C_2T_x$-TiN and maintaining its original 2D structure. In addition, thanks to excellent electronic structure of TiN (001), ultrathin heterostructured nanosheets with a thickness of only a few nanometers significantly shortened electron transfer path and exposed rich adsorption and catalytic active sites. MXene-TiN was mixed with sulfur by a mass ratio of 1:3. The mixture was sealed into a glass bottle filled with Ar gas. Then, the bottle was heated at 155 °C for 15 h to obtain S/MXene-TiN composite. The S content in S/MXene-TiN composite was 73.7 wt%. LSBs with S/MX-TiN cathodes exhibited excellent cycle stability, getting a capacity decay rate of 0.022% per cycle after 1,000 cycles. They also had good electrochemical reversibility under relatively high sulfur loading [Figure 8C and D][99]. In addition, Li *et al.* obtained MXene@$CoSe_2$/N-doped carbon (NC) heterostructured composite material after $CoSe_2$ nanoparticles derived from metal-organic framework were embedded into NC layered MXene HSs [Figure 8E][100]. SEM and transmission electron microscopy (TEM) images displayed that the original sphere and HS skeleton were retained after annealing. At the same time, it

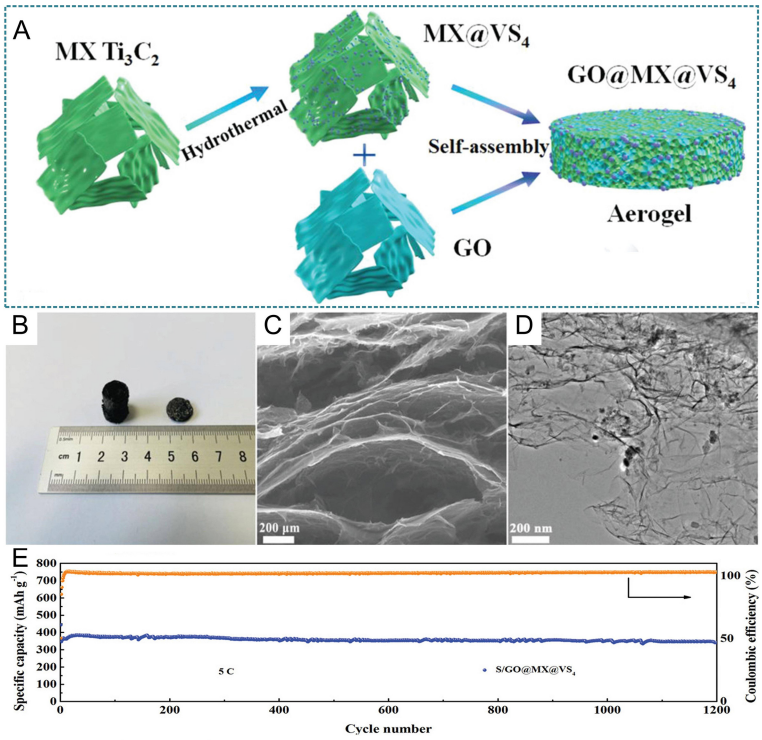

Figure 7. (A) Illustration of synthesis process of GO@MX@VS_4 aerogel. (B) Photo of GO@MX@VS_4 aerogel and self-supporting electrode. (C) SEM and (D) TEM images of GO@MX@VS_4.(E) Long cycle life of S/GO@MX@VS_4 aerogel electrode at 5 C. Reproduced from Ref.[95] with permission from WILEY-VCH.

was seen that $CoSe_2$/NC nanoparticles were distributed on MXene HS [Figure 8F and G]. Therefore, MXene@$CoSe_2$/NC cathodes present excellent electrochemical performance. As shown in Figure 8H, when sulfur loading was 3.5 mg cm^{-2}, a high area specific capacity of 3.343 mAh cm^{-2} was received, and even when facing a low electrolyte/sulfur (E/S) ratio of 5 μL mg^{-1} at 0.2 C, LSBs could still stably circulate for 50 times [Figure 8I].

In summary, there are several types of applications of MXenes in the sulfur cathode of LSBs, which contain directly used MXenes, composite with porous carbons, and composite with heteroatoms and metal compounds. Among them, combining MXenes and metal compounds has turned in a promising direction in recent years, not only inhibiting the stacking of MXene layers but also generating a strong chemical interaction with LiPSs[98]. MXenes and metal compound composite materials are expected to combine excellent anchoring ability and catalytic conversion ability for LiPSs, effectively suppressing the shuttle effect and achieving the excellent electrochemical performance. Consequently, the composites of MXenes and metal compounds are considered the potential sulfur cathodes for LSBs.

Development of MXenes in separators

The porous polypropylene (PP) separator is also an important component of LSBs. During charging and discharging of LSBs, LiPSs cross the separator, causing a shuttle effect, which not only cuts down Coulombic efficiency but also leads to adverse reaction with the lithium anode[101]. By modifying pure PP with various functional materials, LiPSs can be physically or chemically anchored to improve its electrochemical performance[3,102]. Fortunately, the metal atoms in MXenes can strongly interact with LiPSs, effectively suppressing shuttle effect[73]. In addition, the good conductivity and mechanical properties of MXenes facilitate uniform transfer of lithium ions/electrons and overcome volume fluctuation. Meanwhile,

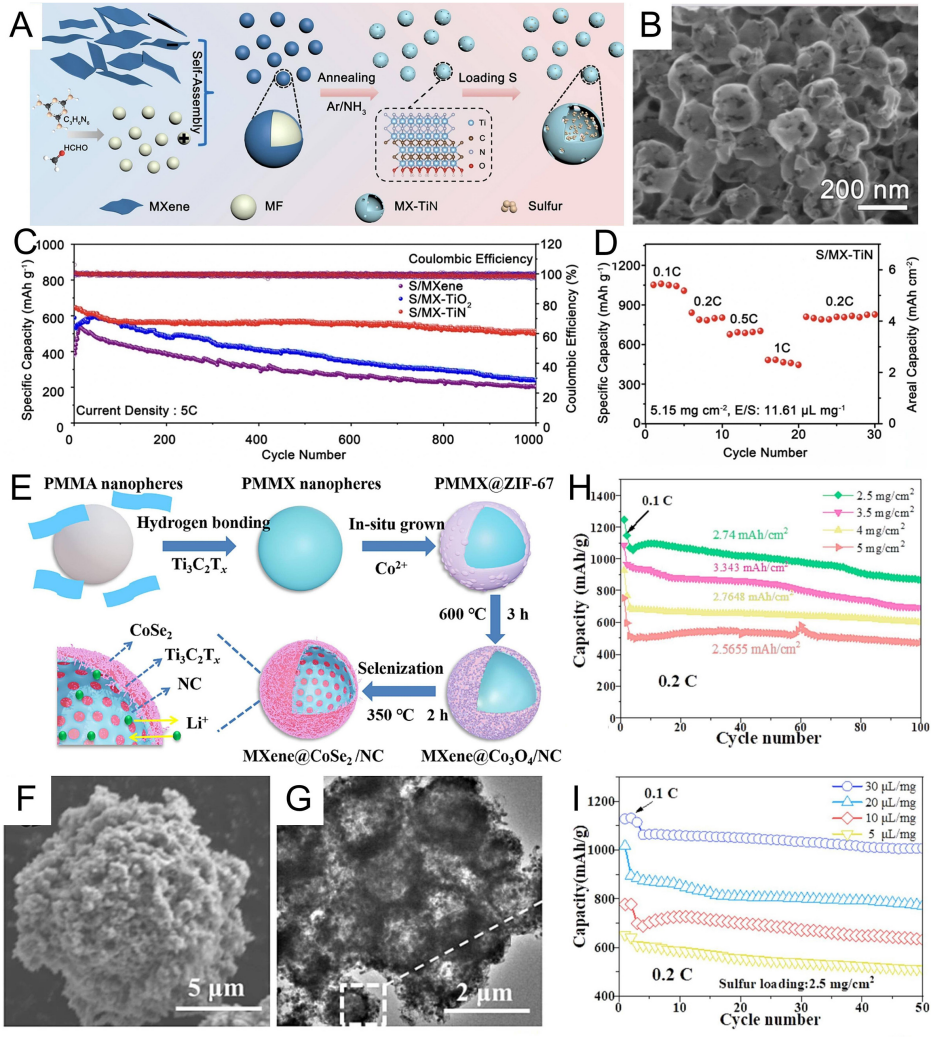

Figure 8. (A) Schematic preparation of MX-TiN and S/MX-TiN hybrid. (B) SEM image of MX-TiN. (C) Long cycle performance of S/MXene, S/MX-TiO_2, and S/MX-TiN cathodes at 5 C. (D) Rate capability of S/MX-TiN at high sulfur loading of 5.15 mg cm^{-2} and E/S ratio of 11.61. Reproduced from Ref.[99] with permission from Springer. (E) Synthetic schematic of MXene@$CoSe_2$/NC. (F) SEM and (G) TEM images of MXene@$CoSe_2$/NC hollow spheres. (H) Cycle performance of LSBs equipped with MXene@$CoSe_2$/NC with different sulfur loadings. (I) Cycle life of LSBs with MXene@$CoSe_2$/NC with different E/S ratios. Reproduced from Ref.[100] with permission from Elsevier.

benefiting from its abundant terminals, the initial nucleation energy of lithium is effectively reduced, thereby inducing the planar deposition[103,104]. These advantages make MXenes stand out among numerous separator modification materials.

Through DFT calculations, Yu *et al.* predicted that $V_4C_3T_x$ had good advantages in promoting the "adsorption-diffusion-conversion" process of LiPSs[105]. Inspired by this, $V_4C_3T_x$ MXene was synthesized through hydrofluoric acid etching and used as a modification layer for PP separators. A $V_4C_3T_x$-PP separator was obtained through the slurry-coating approach. The slurry containing $V_4C_3T_x$, conductive carbon, and polyvinylidene fluoride (PVDF) was dispersed in N-methylpyrrolidone (NMP) at a certain ratio of 70:20:10. Consistent with the calculated results, $V_4C_3T_x$-modified PP separators ($V_4C_3T_x$-PP) blocked and chemically adsorbed LiPSs and effectively catalyzed the conversion of LiPSs. Therefore, LSBs with $V_4C_3T_x$-PP separators exhibited good electrochemical performance. Even when the sulfur loading was

4 mg cm^{-2}, a high area capacity of 4.3 mAh cm^{-2} was still received. In addition, $Ti_3C_2T_x$/CNTs 10% modified PP separators bridged by ultra-light CNTs have been successfully utilized in LSBs. $T_3C_2T_x$ (0.225 mg) and CNT (0.025 mg) were dispersed in a mixed solution of distilled water/ethanol, sonicated, followed by vacuum filtration to obtain the functionalized $Ti_3C_2T_x$-PP. The introduction of CNTs in the $Ti_3C_2T_x$ phase further improves the conductivity of composite material, enhances the specific surface area of the membrane, and improves wettability of the electrolyte. Meanwhile, research has found that reducing the thickness of the modification layer can shorten the transport path of lithium ions. Even under 0.016 mg cm^{-2}, for $Ti_3C_2T_x$-PP separators, the shuttle effect of LiPSs was effectively inhibited[106]. Other modification layers based on carbon materials compounded MXenes have also been widely studied for modifying separators, including porous MXene (PM)-CNT[107], $Ti_3C_2T_x$/GO[108], DNA-CNT/MXene[109], N-Ti_3C_2/C[53], and carbon-coated nitrogen, vanadium co-doped MXene (CNVM)[110]. Interestingly, Gu *et al.* used a vacancy-assisted method to obtain various metal SA catalysts anchored on nitrogen-doped $Ti_3C_2T_x$ (M SA/N-$Ti_3C_2T_x$, M = Cu, Co, Ni, Mn, Zn, In, Sn, Pb, Bi) [Figure 9A][111]. The as-prepared Cu SA/N-$Ti_3C_2T_x$ presented the thin layered morphology; energy-dispersive X-ray spectroscopy (EDS) mapping images showed that Cu and N elements were uniformly distributed on the $Ti_3C_2T_x$ substrate [Figure 9B-D]. The Cu SA/N-$Ti_3C_2T_x$ was applied to the modification layer of PP separators prepared by coating the slurry on PP at a mass ratio of 7:2:1 (catalyst, super P, and PVDF). The testing results demonstrated that compared to pure MXene, N-$Ti_3C_2T_x$ doped with SAs effectively promoted adsorption and kinetic transformation of LiPSs. At the same time, the nitrogen in M SA/N-$Ti_3C_2T_x$ played a key role in regulating the electronegativity environment and electron distribution. After tested in LSBs, Cu SA/N-$Ti_3C_2T_x$/PP possessed a promising cycle life over 1,000 long cycles [Figure 9E].

Similarly, metal compounds combined with MXenes are also used to modify separators to improve the capture ability for LiPSs and accelerate redox kinetics of LiPSs. Chen *et al.* prepared VS_4/$Ti_3C_2T_x$ composite using the simple hydrothermal reaction[112]. The modified separator was acquired using vacuum filtration technology. The solution was obtained by ultrasonic dispersion of (VS_4/$Ti_3C_2T_x$ or VS_4) and LA133 in a mass ratio of 9:1 into a water/ethanol mixture. According to SEM images of VS_4/$Ti_3C_2T_x$, VS_4 attached to $Ti_3C_2T_x$ nanosheets displayed chain-like morphology and "walnut"-shaped submicron spheres (~500 nm) [Figure 10A and B]. A TEM image also confirmed this result [Figure 10C]. VS_4 nanoparticles were uniformly loaded onto thin $Ti_3C_2T_x$ nanosheets. This external load effectively prevented re-accumulation of $Ti_3C_2T_x$. In addition, the unique 3D heterostructure of VS_4/$Ti_3C_2T_x$ shortened the path for Li^+ diffusion and electron transfer. The synergistic effect of VS_4 and $Ti_3C_2T_x$ effectively eased the shuttle of LiPSs and enhanced their catalytic conversion, thereby improving the electrochemical performance of batteries. A strategy for *in-situ* construction of twinborn heterostructures was explored to obtain Ta_4C_3-Ta_2O_5 composite material. Multilayer Ta_4C_3 (m-$Ta_4C_3T_x$) was synthesized by etching an Al layer in Ta_4AlC_3. Subsequently, after undergoing high-temperature calcination in an Ar/H_2 atmosphere, quantum dot-sized Ta_2O_5 particles were formed onto the Ta_4C_3 surface, along with retained 2D structure of a carbon layer. Firstly, Ta_4C_3-Ta_2O_5 and BP 2000 powder were mixed in a ratio of 1:1, followed by adding PVDF at around 10% of the total weight of the two. Finally, slurry was achieved by dispersion in NMP and coated onto PP to get Ta_4C_3-Ta_2O_5@C-PP. When applying Ta_4C_3-Ta_2O_5 to separator modification of LSBs, benefiting from the combination of good conductivity of Ta_4C_3 and strong adsorption of Ta_2O_5 for LiPSs, the battery equipped with a Ta_4C_3-Ta_2O_5@C-PP separator presented high reversible capacity and long cycle life[113]. Tian *et al.* reported MCCoS composite material as a functional layer of separator for LSBs containing alkali etched MXene nanosheets with CoS_2 nanoparticles and CNTs[114]. First, 10 mg $Ti_3C_2T_x$ was added into 20 mL isopropanol and sonicated. Then, a 2.5% mass fraction adhesive (PVDF dissolved in NMP) was added into the above solution and sonicated. Finally, the functionalized MCCoS/PP was prepared by vacuum filtration. As one of the modified material components, the MXene nanosheets not only inhibited the shuttle of LiPSs but also prevented the aggregation and collapse of CoS_2 nanoparticles in LiPSs conversion. Compared with

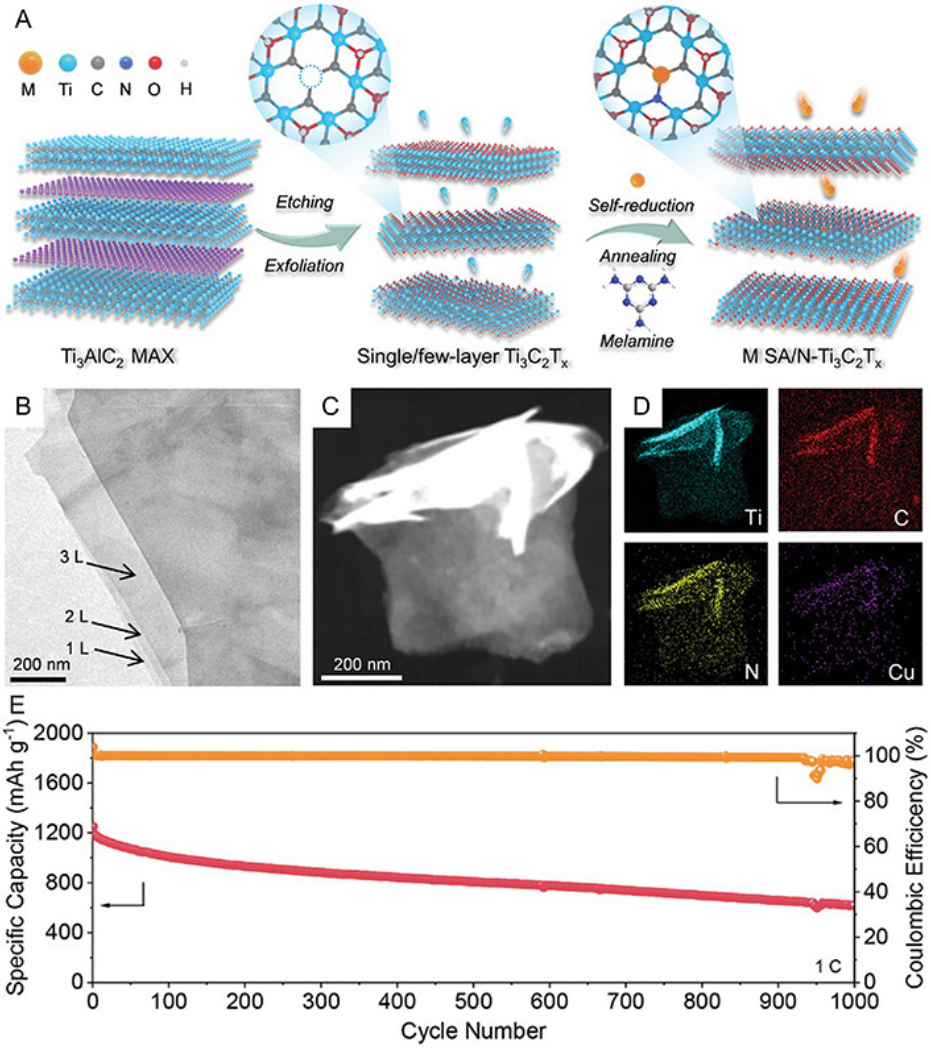

Figure 9. (A) Schematic illustration of M SA/N-$Ti_3C_2T_x$. (B) TEM image of Cu SA/N-$Ti_3C_2T_x$. (C) HAADF-STEM and corresponding (D) EDS mapping images (Ti: cyan; C: red; N: yellow; Cu: purple) of Cu SA/N-$Ti_3C_2T_x$. (E) Cycle life of lithium-sulfur battery based on Cu SA/N-$Ti_3C_2T_x$/PP at 1 C. Reproduced from Ref.[111] with permission from WILEY-VCH.

pure MXene nanosheets [Figure 10D], CoS_2 nanoparticles were uniformly distributed in MXene@CoS_2 composite. However, due to small particle size of CoS_2 [Figure 10E and F], it was difficult to serve as a substrate to prevent MXene nanosheets from stacking. At this point, introducing CNTs precisely solved this difficulty and accelerated the rapid transport of Li^+. Finally, LSBs based on MCCoS/PP separators showed a satisfactory cycling performance at 7 C, including a high first discharge capacity of 698.1 mAh g^{-1}, low decay rate per cycle of 0.033%, and high Coulombic efficiency of 99%-100% after 1,000 cycles [Figure 10G]. The composites of other metal compounds with MXenes as modification layers of separators for LSBs have also been discussed, such as hierarchical porous carbon aerogels embedded with small-sized TiO_2 nanoparticles (HPCA-TO)[115], MXene@WS_2[116], HE-MXene doped graphene composite (HE-MXene/G)[117], and Co_3Se_4 nanoparticles embedded in nitrogen-doped porous carbon/$Ti_3C_2T_x$ (Co_3Se_4@N-C/$Ti_3C_2T_x$)[118].

Development of MXenes in anodes

During charging and discharging of LSBs, the inhomogeneous deposition of metallic lithium leads to the growth of lithium dendrites, seriously affecting their cycling stability. To solve the problem of dendrite in

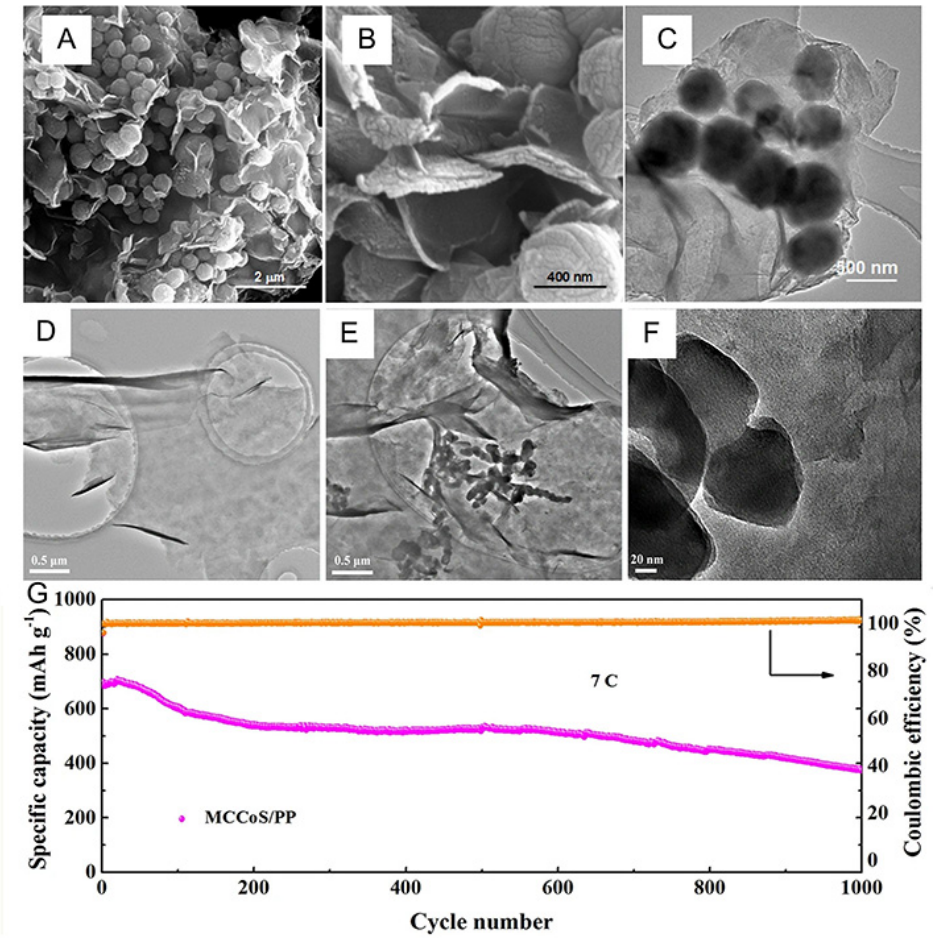

Figure 10. (A and B) SEM and (C) TEM images of $VS_4/Ti_3C_2T_x$ composite. Reproduced from Ref.[112] with permission from Elsevier. (D) TEM image of MX. (E and F) TEM images of MX@CoS_2. (G) Long cycle life of MCCoS/PP separator-based lithium-sulfur battery at 7 C. Reproduced from Ref.[114] with permission from Springer.

lithium anode, Li *et al.* prepared MXene (graphene, BN)-lithium film anode using a mechanical rolling method based on the extensibility of metallic lithium[119]. In the as-obtained flexible film, lithiophobic atomic layers acted as "artificial solid electrolyte interphase films" of metallic lithium and maintained stability during the repeated stripping and plating processes of lithium anode. As a result, a LSB with Ti_3C_2-Li as an anode and sulfur-carbon as a cathode possessed a high energy density of 656 Wh kg^{-1}. In addition, Li *et al.* combined reduced GO (rGO) with $Ti_3C_2T_x$ to form a layered composite for lithium anode modification[120]. Figure 11A shows the process of forming Li-rGO/$Ti_3C_2T_x$ composite anode by injecting molten lithium into rGO/$Ti_3C_2T_x$ film. Even at 10 mA cm^{-2} and 3 mAh cm^{-2}, the symmetric battery with Li-rGO/$Ti_3C_2T_x$ exhibited excellent cycling stability for over 1,000 h [Figure 11B]. In a lithium-sulfur full battery, the composite anode effectively eased the shuttle of LiPSs and inhibited formation of lithium dendrites. Therefore, a capacity retention rate of 64.5% and a high Coulombic efficiency of 99.8% were acquired after 300 cycles [Figure 11C].

More interestingly, Wei *et al.* reported a versatile 3D printed (3DP) nitrogen-doped porous Ti_3C_2 MXene framework (*N*-p$Ti_3C_2T_x$), which was simultaneously used as both a sulfur carrier and a lithium anode modification layer for a LSB [Figure 11D][121]. At 5.0 mA cm^{-2} and 5.0 mAh cm^{-2}, the cycle life of a symmetrical cell reached 800 h [Figure 11E]. Figure 11F demonstrates that lithium-sulfur full battery based

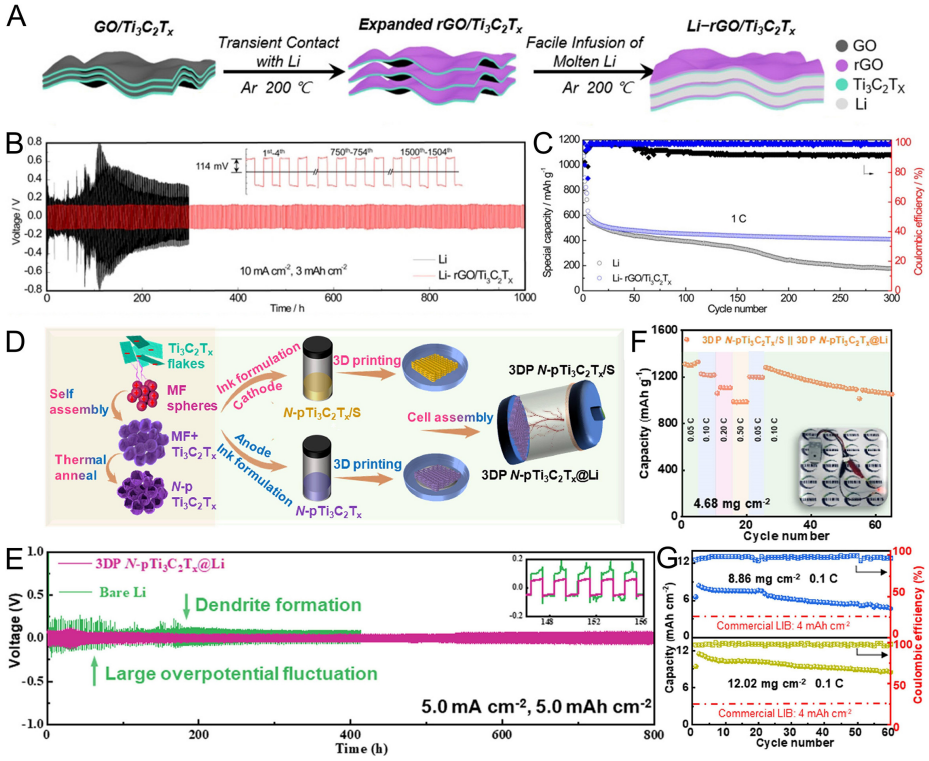

Figure 11. (A) Scheme for synthesis of layered Li-rGO/$Ti_3C_2T_x$ composite anode. (B) Cycling performance of symmetric batteries based on Li-rGO/$Ti_3C_2T_x$ and bare Li electrodes under 10 mA cm^{-2}/3 mAh cm^{-2}. (C) Cycling performance of LSBs based on bare Li metal and Li-rGO/$Ti_3C_2T_x$ anodes at 1 C. Reproduced from Ref.[120] with permission from WILEY-VCH. (D) Schematic diagram of preparation process of LSB dual electrodes based on 3DP *N*-p$Ti_3C_2T_x$ framework. (E) Cyclic performance of symmetric cells at 5.0 mA cm^{-2}/5.0 mAh cm^{-2}. Inset: the selective voltage-time profiles for corresponding symmetric cells. (F) Rate performance of 3DP *N*-p$Ti_3C_2T_x$/S||3DP *N*-p$Ti_3C_2T_x$@Li lithium-sulfur full battery. Inset: LSB full cell powering a red LED indicator (E/S ratio: 9 μL mg^{-1}). (G) Cyclic life of 3DP *N*-p$Ti_3C_2T_x$/S||3DP *N*-p$Ti_3C_2T_x$@Li LSB full cells at 0.1 C at different sulfur loadings (E/S ratio: 5 μL mg^{-1}). Reproduced from Ref.[121] with permission from Elsevier.

on 3DP *N*-p$Ti_3C_2T_x$/S cathode and *N*-p$Ti_3C_2T_x$@Li anode possesses excellent rate performance with a sulfur loading of 4.68 mg cm^{-2}. More importantly, under the conditions of 8.86 and 12.02 mg cm^{-2}, the satisfactory reversible capacities were still achieved after 60 cycles [Figure 11G]. A lithiophilic 3D MXene/graphene (MG) framework was reported. Thanks to a large specific surface area (259 m^2 g^{-1}) and lightweight nature, MG-based electrodes had a high Coulombic efficiency (~99%) and an ultra-long lifespan (2,700 h), and MG-lithium/sulfur batteries show good rate performance, meaning that this 3D MG framework possesses potential advantages for obtaining long-lived high-energy-density LSBs[122]. In addition, other materials containing MXenes are also utilized for modifying lithium metal anodes, including Ti_3C_2/CoP nanocages (CPNC)[123], ZnS/MXene[124], $CoSe_2$@N-MXene film (NMF)[125], halogenated MXenes[126], and MXene@Ag[127].

Development of MXenes in electrolytes

Thanks to the abundant polar groups on the surface, the applications of MXenes in electrolytes have also been developed[128,129]. Liu *et al.* reported a quasi-solid-state anode-free battery assembled by a high-capacity Li_2S cathode and a composite gel polymer electrolyte (CGPE)[128]. The CGPE comprised poly(vinylidene fluoride-co-hexafluoropropylene), $Ti_3C_2T_x$ MXene, and lithium bis(trifluoromethanesulphonyl)imide. The introduction of MXene not only accelerated the dissociation and transformation of Li_2S but also contributed to rapid ion transport, good flame retardancy, and thermal stability of gel electrolyte. Importantly, MXene-

doped gel electrolyte effectively inhibited the shuttle of LiPSs and prevented the formation of lithium dendrites. Therefore, the quasi-solid-state anode-free battery with CGPE exhibited good reversibility and high energy density. In addition, Liu *et al.* reasonably proposed "a two birds with one stone strategy" and successfully received Nb_2CT_x MXene-integrated polyethylene oxide-based polymer electrolyte for all-solid-state LSBs[129]. Firstly, Nb_2CT_x nanosheets were obtained using an acid etching of Nb_2AlC and tetrapropylammonium hydroxide intercalation/ultrasound method. It was found that when the sheet size was adjusted below 100 nm, the interaction between polyethylene oxide matrix and Nb_2CT_x MXene interface improved Li^+ conductivity and adsorption of LiPSs. After adjustment, the ion conductivity increased from 8.56×10^{-5} to 2.62×10^{-4} S cm^{-1} at 60 °C. Thus, the all-solid-state LSB delivered an initial capacity of 1,149 mAh g^{-1} at 0.5 C and cycled over 200 cycles. This work also offers an idea for further applying MXenes in electrolytes for solid-state LSBs.

In a word, MXenes are used in four aspects, including cathodes, separators, anodes, and electrolytes, for LSBs. A brief summary of comparison of different works on using MXenes for LSBs is listed in Table 2.

Applications of MXenes in other energy storage/conversion devices

Owing to their excellent metal conductivity, mechanical strength, and abundant surface terminals, MXenes and their composite materials have become the promising direction in the applications of LSBs in recent years. However, in other types of metal-sulfur battery applications, MXenes also demonstrate the outstanding research value. For example, the porous nitrogen-doped $Ti_3C_2T_x$ MXene microspheres prepared as the sulfur cathode for long-life room temperature sodium-sulfur battery delivered the reversible capacity of 980 mAh g^{-1} at 0.5 C[130]. The applications of MXenes in other types of batteries are also studied, such as sodium-ion[131], potassium-ion[132], Li-O_2[133], Zn-air[134], and other batteries.

PERSPECTIVE AND OUTLOOK

LSBs have made the significant progress since their invention. In the meantime, the various materials are applied to LSBs. This article reviews the characteristics and synthesis methods of MXenes and briefly overviews their application in LSBs. MXenes, due to their structural diversity, excellent conductivity, and high mechanical strength, show promising potential for application in high-performance LSBs. When used in cathodes and separators for LSBs, their surface-rich metal sites and functional groups enhance adsorption of LiPSs and accelerate their catalytic conversion, effectively suppressing the shuttle effect[73]. Additionally, because of high conductivity and mechanical properties, MXenes exhibit the great advantages in the uniform transmission of lithium ions/electrons and overcoming the volume fluctuation. Meanwhile, when used to modify lithium anodes, they benefit from the abundant terminals and effectively reduce the initial nucleation energy of lithium, thereby inducing the even deposition of lithium and suppressing the formation of lithium dendrites[103,104]. It is evident that MXenes have made the significant progress in the development of LSBs; future research should focus on the following aspects and address the technical challenges to better align with the practical application:

(1) HF and F-based salt etching methods for preparing MXenes are still commonly chosen by researchers, but these two methods inevitably pollute the environment and pose safety hazards. Therefore, some environmentally friendly techniques need to be further explored. In addition, HF and F-based salt etching techniques introduce terminals such as -O, -OH, and -F. However, F-terminated MXenes are detrimental to the electrochemical performance[23,135]. The recent Lewis acid MS etching approach stands out because it can selectively regulate and obtain the fluorine-free surface terminals[25].

Table 2. Comparison of different works on using MXenes for LSBs

Material	Category	Current density	Cycle number	Capacity (mA h g^{-1})	Ref.
$Ti_3C_2T_x$ paper	Cathode	1 C	1,500	970	[77]
MS-$Ti_3C_2T_x$-600	Cathode	0.1 C	100	752	[78]
Ff-Ti_3C_2	Cathode	1 C	500	585	[79]
$Ti_3C_2T_x$/RGO	Cathode	0.5 C	300	878.4	[81]
MG/C_3N_4	Cathode	2 C	250	1,010.8	[83]
CNT-MXene	Cathode	0.5 C	1,200	~450	[84]
Mo_2C-CNT	Cathode	1 C	100	~954	[85]
GM0.4	Cathode	0.5 C	1,000	542.9	[86]
KB@$Ti_3C_2T_x$	Cathode	0.5 C	400	-	[87]
N-Ti_3C_2@CNTs	Cathode	1 C	1,000	775.6	[88]
P-NTC	Cathode	2 C	1,200	-	[89]
N-$Ti_3C_2T_x$	Cathode	2 C	1,000	610	[90]
NMSG-1.5	Cathode	1 C	300	721.7	[91]
SA-Zn-MXene	Cathode	1 C	400	706	[92]
V_3S_4@C-7	Cathode	2 C	1,000	~532.1	[94]
GO@MX@VS_4	Cathode	5 C	1,200	-	[95]
Nb_2C/Nb_2O_5	Cathode	1 C	500	621	[96]
OV-T_nQDs@PCN	Cathode	2 C	1,000	660	[97]
TiN@MXene	Cathode	1 C	1,000	474	[98]
MX-TiN	Cathode	5 C	1,000	516.9	[99]
MXene@$CoSe_2$/NC	Cathode	1 C	800	-	[100]
$CoSe_2$@$TiSe_2$-C	Separator	1 C	800	842.4	[102]
T@CP	Cathode Separator	1 C	500	980	[103]
$V_4C_3T_x$	Separator	1 C	800	516	[105]
$Ti_3C_2T_x$/CNTs 10%	Separator	1 C	200	-	[106]
PM (0.4 M)-CNT	Separator	1 C	500	535	[107]
$Ti_3C_2T_x$/GO	Separator	1 C	300	-	[108]
DNA-CNT/MXene	Separator	1 C	200	592	[109]
CNVM	Separator	1 C	660	440	[110]
Cu SA/N-$Ti_3C_2T_x$	Separator	2 C	400	736	[111]
$VS_4/Ti_3C_2T_x$	Separator	1 C	500	657	[112]
Ta_4C_3-Ta_2O_5@C	Separator	1 C	500	-	[113]
MCCoS	Separator	7 C	1,000	-	[114]
HPCA-TO	Separator	1 C	200	513	[115]
MXene@WS_2	Separator	2 C	2,000	380.5	[116]
HE-MXene/G	Separator	1 C	1,200	654.8	[117]
Co_3Se_4@N-C/$Ti_3C_2T_x$	Separator	2 C	300	607	[118]
Ti_3C_2	Anode	0.12 C	200	~750	[119]
rGO/$Ti_3C_2T_x$	Anode	1 C	300	409	[120]
3DP *N*-p$Ti_3C_2T_x$	Cathode Anode	1 C	150	-	[121]
MG	Anode	0.5 C	300	-	[122]
Ti_3C_2/CPNC	Separator Anode	0.5 C	250	520	[123]
ZM-C	Anode	1 C	250	671.2	[124]
$CoSe_2$@NMF	Anode	0.2 C	100	610.5	[125]
CGPE	Electrolyte	233.2 mA g^{-1}	300	-	[128]
PEO/LiTFSI-S3	Electrolyte	0.5 C	200	491	[129]

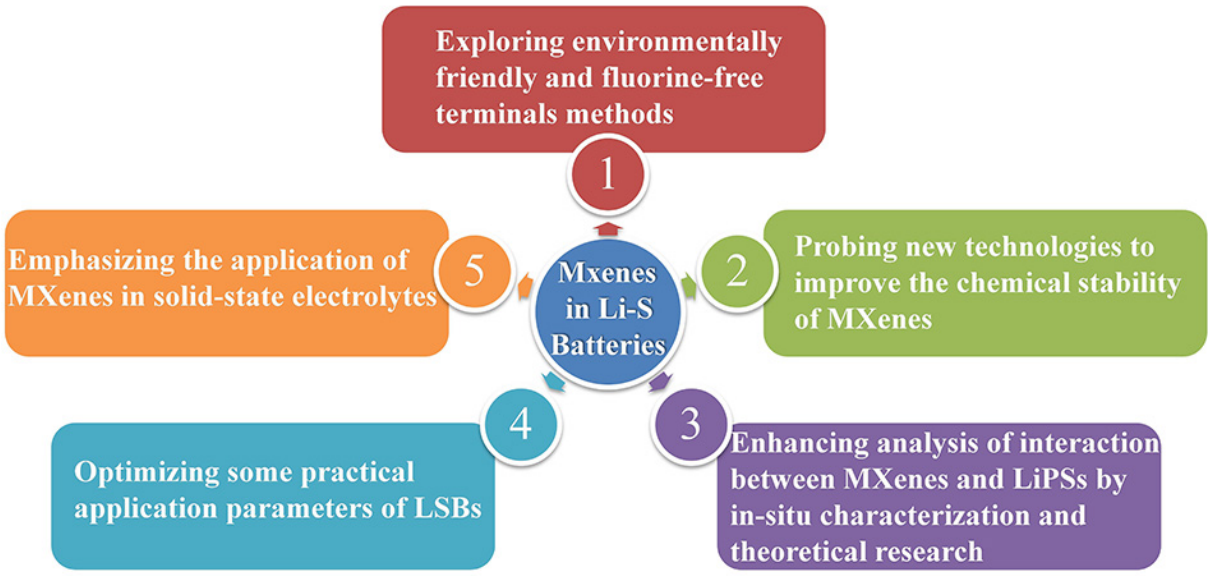

Figure 12. Perspective and outlook of MXenes-based LSBs.

(2) The chemical stability of MXenes significantly influences their application in LSBs. They are highly susceptible to oxidation in humid air. Low temperature, addition of antioxidants, and hydrogen annealing significantly improve the chemical stability. However, in addition to the harsh environmental conditions, the material after hydrogen treatment has a poor redispersibility, and the introduction of a large number of insulation additives reduces the conductivity and chemical compatibility of MXenes, thereby affecting the battery performance[39-42,136]. Thus, it is necessary to explore new technologies to guarantee the improvement in chemical stability of MXenes while ensuring that the electrochemical performance is unaffected.

(3) MXene nanosheets are prone to stacking because of strong van der Waals force. The composite of MXenes with other materials not only effectively avoids the restacking of MXene nanosheets but also further improves the electrochemical performance. Recently, it has been found that the composites of MXenes with other metal compounds or *in-situ* transformation of MXenes to form composite materials with heterostructures exhibit conspicuous potential. However, due to the complex chemical reactions during charging/discharging of LSBs, the interaction between MXene and LiPS needs to be further groped. Some *in-situ* characterization tests should be combined to provide a more detailed explanation of reaction mechanisms. Combining theoretical and experimental research can provide a more comprehensive understanding of reaction mechanisms and pathways.

(4) Some parameters of LSBs, including the area load of sulfur, the content of sulfur in the cathode, the E/S ratio, and the excess mass of lithium, significantly influence the energy density[3]. However, the parameter values mentioned above in the current reports are far from practical application. In the future, much effort should be made to explore the electrochemical performance under high sulfur content, moderate lithium mass, and low E/S ratio to commercialize LSBs.

(5) From the application perspective of LSBs, the current research on MXenes mainly focuses on sulfur cathodes, functional separators, and modification of lithium metal anodes, while solid-state electrolytes are very scarce. Considering the excellent characteristics of MXenes, more attention should be paid to their use in solid-state electrolytes in the future.

Although dozens of MXenes have been successfully prepared so far, according to our summary, their types utilized in LSBs are very limited. We hope that more types can be developed for high-performance LSBs. We believe that in the near future, MXenes in the field of LSBs will have "a hundred flowers blooming and a hundred schools of thought competing". Figure 12 shows the perspective and outlook of MXenes-based LSBs.

DECLARATIONS

Authors' contributions

Proposed the topic of this review: Jin B
Prepared the manuscript: Liu H, Sun ST
Collectively discussed and revised the manuscript: Liu H, Jin B

Availability of data and materials

Not applicable.

Financial support and sponsorship

This work was supported by the National Natural Science Foundation of China (No. 52130101) and the Project of Science and Technology Development Plan of Jilin Province in China (Nos. 20210402058GH and 20220201114GX).

Conflicts of interest

All authors declared that there are no conflicts of interest.

Ethical approval and consent to participate

Not applicable.

Consent for publication

Not applicable.

REFERENCES

1. Armand M, Tarascon JM. Building better batteries. *Nature* 2008;451:652-7. DOI PubMed
2. Dunn B, Kamath H, Tarascon JM. Electrical energy storage for the grid: a battery of choices. *Science* 2011;334:928-35. DOI PubMed
3. Peng H, Huang J, Cheng X, Zhang Q. Review on high-loading and high-energy lithium-sulfur batteries. *Adv Energy Mater* 2017;7:1700260. DOI
4. Huang S, Huixiang E, Yang Y, Zhang Y, Ye M, Li CC. Transition metal phosphides: new generation cathode host/separator modifier for Li-S batteries. *J Mater Chem A* 2021;9:7458-80. DOI
5. Liu B, Zhang J, Xu W. Advancing lithium metal batteries. *Joule* 2018;2:833-45. DOI
6. Li H, Zhao M, Jin B, Wen Z, Liu HK, Jiang Q. Mesoporous nitrogen-doped carbon nanospheres as sulfur matrix and a novel chelate-modified separator for high-performance room-temperature Na-S batteries. *Small* 2020;16:e1907464. DOI
7. Dong C, Zhou H, Liu H, et al. Inhibited shuttle effect by functional separator for room-temperature sodium-sulfur batteries. *J Mater Sci Technol* 2022;113:207-16. DOI
8. Wang Y, Meng Y, Zhang Z, Guo Y, Xiao D. Trifunctional electrolyte additive hexadecyltrioctylammonium iodide for lithium-sulfur batteries with extended cycle life. *ACS Appl Mater Interfaces* 2021;13:16545-57. DOI
9. Wu DS, Shi F, Zhou G, et al. Quantitative investigation of polysulfide adsorption capability of candidate materials for Li-S batteries. *Energy Storage Mater* 2018;13:241-6. DOI

10. Seh ZW, Sun Y, Zhang Q, Cui Y. Designing high-energy lithium-sulfur batteries. *Chem Soc Rev* 2016;45:5605-34. DOI
11. Yin YX, Xin S, Guo YG, Wan LJ. Lithium-sulfur batteries: electrochemistry, materials, and prospects. *Angew Chem Int Ed* 2013;52:13186-200. DOI PubMed
12. Wang D, Zeng Q, Zhou G, et al. Carbon-sulfur composites for Li-S batteries: status and prospects. *J Mater Chem A* 2013;1:9382. DOI
13. Chung SH, Manthiram A. Current status and future prospects of metal-sulfur batteries. *Adv Mater* 2019;31:e1901125. DOI PubMed
14. Zheng J, Lv D, Gu M, et al. How to obtain reproducible results for lithium sulfur batteries? *J Electrochem Soc* 2013;160:A2288-92. DOI
15. Xu J, Xu L, Zhang Z, et al. Heterostructure ZnSe-$CoSe_2$ embedded with yolk-shell conductive dodecahedral as two-in-one hosts for cathode and anode protection of lithium-sulfur full batteries. *Energy Storage Mater* 2022;47:223-34. DOI
16. Sheng Q, Liu H, Liu Y, et al. Functional separator with 1T/2H-$MoSe_2$ nanosheets decorated nitrogen and sulfur co-doped mesoporous hollow carbon spheres for high-performance Li-S batteries. *Chem Eng J* 2023;476:146880. DOI
17. Yao W, Xu J, Ma L, et al. Recent progress for concurrent realization of shuttle-inhibition and dendrite-free lithium-sulfur batteries. *Adv Mater* 2023;35:e2212116. DOI
18. Li H, Zhou Y, Zhao M, et al. Suppressed shuttle via inhibiting the formation of long-chain lithium polysulfides and functional separator for greatly improved lithium-organosulfur batteries performance. *Adv Energy Mater* 2020;10:1902695. DOI
19. Wu H, Gao X, Chen X, et al. Dual-single-atoms of Pt-Co boost sulfur redox kinetics for ultrafast Li-S batteries. *Carbon Energy* 2024;6:e422. DOI
20. Han SA, Qutaish H, Lee J, Park M, Kim JH. Metal-organic framework derived porous structures towards lithium rechargeable batteries. *EcoMat* 2023;5:e12283. DOI
21. Xiao Z, Li Z, Meng X, Wang R. MXene-engineered lithium-sulfur batteries. *J Mater Chem A* 2019;7:22730-43. DOI
22. Deysher G, Shuck CE, Hantanasirisakul K, et al. Synthesis of Mo_4VAlC_4 MAX phase and two-dimensional Mo_4VC_4 MXene with five atomic layers of transition metals. *ACS Nano* 2020;14:204-17. DOI
23. Wei Y, Zhang P, Soomro RA, Zhu Q, Xu B. Advances in the synthesis of 2D MXenes. *Adv Mater* 2021;33:e2103148. DOI
24. VahidMohammadi A, Rosen J, Gogotsi Y. The world of two-dimensional carbides and nitrides (MXenes). *Science* 2021;372:eabf1581. DOI PubMed
25. An Y, Tian Y, Shen H, Man Q, Xiong S, Feng J. Two-dimensional MXenes for flexible energy storage devices. *Energy Environ Sci* 2023;16:4191-250. DOI
26. Naguib M, Kurtoglu M, Presser V, et al. Two-dimensional nanocrystals produced by exfoliation of Ti_3AlC_2. *Adv Mater* 2011;23:4248-53. DOI
27. Anasori B, Lukatskaya MR, Gogotsi Y. 2D metal carbides and nitrides (MXenes) for energy storage. *Nat Rev Mater* 2017;2:16098. DOI
28. Lai S, Jeon J, Jang SK, et al. Surface group modification and carrier transport properties of layered transition metal carbides (Ti_2CT_x, T: -OH, -F and -O). *Nanoscale* 2015;7:19390-6. DOI
29. Hu T, Wang J, Zhang H, Li Z, Hu M, Wang X. Vibrational properties of Ti_3C_2 and $Ti_3C_2T_2$ (T = O, F, OH) monosheets by first-principles calculations: a comparative study. *Phys Chem Chem Phys* 2015;17:9997-10003. DOI
30. Khazaei M, Arai M, Sasaki T, et al. Novel electronic and magnetic properties of two-dimensional transition metal carbides and nitrides. *Adv Funct Mater* 2013;23:2185-92. DOI
31. Jayan R, Vashisth A, Islam MM. First-principles investigation of elastic and electronic properties of double transition metal carbide MXenes. *J Am Ceram Soc* 2022;105:4400-13. DOI
32. Azadi SK, Zeynali M, Asgharizadeh S, Fooladloo MA. Investigation of the optical and electronic properties of functionalized Ti_3C_2 Mxene with halid atoms using DFT calculation. *Mater Today Commun* 2023;35:106136. DOI
33. Zhang Y, Zha X, Luo K, et al. Theoretical study on the electrical and mechanical properties of MXene multilayer structures through strain regulation. *Chem Phys Lett* 2020;760:137997. DOI
34. Lipatov A, Alhabeb M, Lukatskaya MR, Boson A, Gogotsi Y, Sinitskii A. Effect of synthesis on quality, electronic properties and environmental stability of individual monolayer Ti_3C_2 MXene flakes. *Adv Electron Mater* 2016;2:1600255. DOI
35. Zeraati A, Mirkhani SA, Sun P, Naguib M, Braun PV, Sundararaj U. Improved synthesis of $Ti_3C_2T_x$ MXenes resulting in exceptional electrical conductivity, high synthesis yield, and enhanced capacitance. *Nanoscale* 2021;13:3572-80. DOI PubMed
36. Zhang J, Kong N, Uzun S, et al. Scalable manufacturing of free-standing, strong $Ti_3C_2T_x$ MXene films with outstanding conductivity. *Adv Mater* 2020;32:e2001093. DOI
37. Xue N, Li X, Han L, et al. Fluorine-free synthesis of ambient-stable delaminated Ti_2CT_x (MXene). *J Mater Chem A* 2022;10:7960-7. DOI
38. Mashtalir O, Cook KM, Mochalin VN, Crowe M, Barsoum MW, Gogotsi Y. Dye adsorption and decomposition on two-dimensional titanium carbide in aqueous media. *J Mater Chem A* 2014;2:14334-8. DOI
39. Zhang CJ, Pinilla S, Mcevoy N, et al. Oxidation stability of colloidal two-dimensional titanium carbides (MXenes). *Chem Mater* 2017;29:4848-56. DOI
40. Chae Y, Kim SJ, Cho SY, et al. An investigation into the factors governing the oxidation of two-dimensional Ti_3C_2 MXene. *Nanoscale* 2019;11:8387-93. DOI
41. Echols IJ, Holta DE, Kotasthane VS, et al. Oxidative stability of $Nb_{n+1}C_nT_z$ MXenes. *J Phys Chem C* 2021;125:13990-6. DOI

42. Lee Y, Kim SJ, Kim Y, et al. Oxidation-resistant titanium carbide MXene films. *J Mater Chem A* 2020;8:573-81. DOI
43. Lee DK, Chae Y, Yun H, Ahn CW, Lee JW. CO_2-Oxidized $Ti_3C_2T_x$-MXenes components for lithium-sulfur batteries: suppressing the shuttle phenomenon through physical and chemical adsorption. *ACS Nano* 2020;14:9744-54. DOI
44. Borysiuk VN, Mochalin VN, Gogotsi Y. Molecular dynamic study of the mechanical properties of two-dimensional titanium carbides $Ti_{n+1}C_n$ (MXenes). *Nanotechnology* 2015;26:265705. DOI PubMed
45. Guo Z, Zhou J, Si C, Sun Z. Flexible two-dimensional $Ti_{n+1}C_n$ (n = 1, 2 and 3) and their functionalized MXenes predicted by density functional theories. *Phys Chem Chem Phys* 2015;17:15348-54. DOI PubMed
46. Chen Y, Tang S, Yan X. Manipulating the crack path through the surface functional groups of MXenes. *Nanoscale* 2022;14:14169-77. DOI
47. Pan Y, Fu L, Zhou Q, et al. Flammability, thermal stability and mechanical properties of polyvinyl alcohol nanocomposites reinforced with delaminated $Ti_3C_2T_x$ (MXene). *Polym Compos* 2020;41:210-8. DOI
48. Wan S, Li X, Chen Y, et al. High-strength scalable MXene films through bridging-induced densification. *Science* 2021;374:96-9. DOI
49. Alhabeb M, Maleski K, Anasori B, et al. Guidelines for synthesis and processing of two-dimensional titanium carbide ($Ti_3C_2T_x$ MXene). *Chem Mater* 2017;29:7633-44. DOI
50. Srivastava P, Mishra A, Mizuseki H, Lee KR, Singh AK. Mechanistic insight into the chemical exfoliation and functionalization of Ti_3C_2 MXene. *ACS Appl Mater Interfaces* 2016;8:24256-64. DOI
51. Mashtalir O, Naguib M, Mochalin VN, et al. Intercalation and delamination of layered carbides and carbonitrides. *Nat Commun* 2013;4:1716. DOI
52. Maleski K, Mochalin VN, Gogotsi Y. Dispersions of two-dimensional titanium carbide MXene in organic solvents. *Chem Mater* 2017;29:1632-40. DOI
53. Jiang G, Zheng N, Chen X, et al. In-situ decoration of MOF-derived carbon on nitrogen-doped ultrathin MXene nanosheets to multifunctionalize separators for stable Li-S batteries. *Chem Eng J* 2019;373:1309-18. DOI
54. Li Z, Wang L, Sun D, et al. Synthesis and thermal stability of two-dimensional carbide MXene Ti_3C_2. *Mater Sci Eng B* 2015;191:33-40. DOI
55. Wang K, Zhou Y, Xu W, Huang D, Wang Z, Hong M. Fabrication and thermal stability of two-dimensional carbide Ti_3C_2 nanosheets. *Ceram Int* 2016;42:8419-24. DOI
56. Ghidiu M, Lukatskaya MR, Zhao MQ, Gogotsi Y, Barsoum MW. Conductive two-dimensional titanium carbide 'clay' with high volumetric capacitance. *Nature* 2014;516:78-81. DOI PubMed
57. Ebrahimi M, Mei C. Optoelectronic properties of $Ti_3C_2T_x$ MXene transparent conductive electrodes: microwave synthesis of parent MAX phase. *Ceram Int* 2020;46:28114-9. DOI
58. Li X, Li Q, Hou Y, et al. Toward a practical Zn powder anode: $Ti_3C_2T_x$ MXene as a lattice-match electrons/ions redistributor. *ACS Nano* 2021;15:14631-42. DOI
59. Wu M, Wang B, Hu Q, Wang L, Zhou A. The synthesis process and thermal stability of V_2C MXene. *Materials* 2018;11:2112. DOI PubMed PMC
60. Wang X, Garnero C, Rochard G, et al. A new etching environment (FeF_3 /HCl) for the synthesis of two-dimensional titanium carbide MXenes: a route towards selective reactivity vs. water. *J Mater Chem A* 2017;5:22012-23. DOI
61. Wang B, Zhou A, Liu F, Cao J, Wang L, Hu Q. Carbon dioxide adsorption of two-dimensional carbide MXenes. *J Adv Ceram* 2018;7:237-45. DOI
62. Urbankowski P, Anasori B, Makaryan T, et al. Synthesis of two-dimensional titanium nitride Ti_4N_3 (MXene). *Nanoscale* 2016;8:11385-91. DOI
63. Khan U, Luo Y, Kong LB, Que W. Synthesis of fluorine free MXene through lewis acidic etching for application as electrode of proton supercapacitors. *J Alloys Compd* 2022;926:166903. DOI
64. Kamysbayev V, Filatov AS, Hu H, et al. Covalent surface modifications and superconductivity of two-dimensional metal carbide MXenes. *Science* 2020;369:979-83. DOI
65. Xuan J, Wang Z, Chen Y, et al. Organic-base-driven intercalation and delamination for the production of functionalized titanium carbide nanosheets with superior photothermal therapeutic performance. *Angew Chem Int Ed* 2016;128:14789-94. DOI
66. Li T, Yao L, Liu Q, et al. Fluorine-free synthesis of high-purity $Ti_3C_2T_x$ (T=OH, O) via Alkali Treatment. *Angew Chem Int Ed* 2018;130:6223-7. DOI
67. Chen J, Chen M, Zhou W, et al. Simplified synthesis of fluoride-free $Ti_3C_2T_x$ via electrochemical etching toward high-performance electrochemical capacitors. *ACS Nano* 2022;16:2461-70. DOI
68. Pang SY, Wong YT, Yuan S, et al. Universal strategy for HF-free facile and rapid synthesis of two-dimensional MXenes as multifunctional energy materials. *J Am Chem Soc* 2019;141:9610-6. DOI
69. Wang D, Zhou C, Filatov AS, et al. Direct synthesis and chemical vapor deposition of 2D carbide and nitride MXenes. *Science* 2023;379:1242-7. DOI
70. Shi H, Zhang P, Liu Z, et al. Ambient-stable two-dimensional titanium carbide (MXene) enabled by iodine etching. *Angew Chem Int Ed* 2021;133:8771-5. DOI PubMed PMC
71. Ding J, Zhao H, Wang Q, Dou H, Chen H, Yu H. An ultrahigh thermal conductive graphene flexible paper. *Nanoscale* 2017;9:16871-8. DOI

72. Zhu C, Hui Z, Pan H, et al. Ultrafast Li-ion migration in holey-graphene-based composites constructed by a generalized *ex situ* method towards high capacity energy storage. *J Mater Chem A* 2019;7:4788-96. DOI
73. Xu H, Kong Z, Siegenthaler J, et al. Review on recent advances in two-dimensional nanomaterials-based cathodes for lithium-sulfur batteries. *EcoMat* 2023;5:e12286. DOI
74. Chen X, Li L, Shan Y, Zhou D, Cui W, Zhao Y. Notes in accordions - organized MXene equipped with CeO_2 for synergistically adsorbing and catalyzing polysulfides for high-performance lithium-sulfur batteries. *J Energy Chem* 2022;70:502-10. DOI
75. Liang X, Garsuch A, Nazar LF. Sulfur cathodes based on conductive MXene nanosheets for high-performance lithium-sulfur batteries. *Angew Chem Int Ed* 2015;127:3979-83. DOI PubMed
76. Zhao Y, Li Q, Liu Z, et al. Stable electrochemical Li plating/stripping behavior by anchoring MXene layers on three-dimensional conductive skeletons. *ACS Appl Mater Interfaces* 2020;12:37967-76. DOI
77. Tang H, Li W, Pan L, et al. A robust, freestanding MXene-sulfur conductive paper for long-lifetime Li-S batteries. *Adv Funct Mater* 2019;29:1901907. DOI
78. Yang C, Yu Z, Jian C, Li T, Tian L, Liu H. Molten salt etched $Ti_3C_2T_x$ MXene for ameliorated electrochemical performances of lithium-sulfur batteries. *J Mater Sci Mater Electron* 2023;34:718. DOI
79. Liang L, Niu L, Wu T, Zhou D, Xiao Z. Fluorine-free fabrication of MXene via photo-fenton approach for advanced lithium-sulfur batteries. *ACS Nano* 2022;16:7971-81. DOI PubMed
80. Wang Z, Bai J, Xu H, Chen G, Kang S, Li X. Synthesis of three-dimensional Sn@Ti_3C_2 by layer-by-layer self-assembly for high-performance lithium-ion storage. *J Colloid Interface Sci* 2020;577:329-36. DOI
81. Bao W, Xie X, Xu J, et al. Confined sulfur in 3D MXene/reduced graphene oxide hybrid nanosheets for lithium-sulfur battery. *Chemistry* 2017;23:12613-9. DOI
82. Zhang CF, Cui LF, Abdolhosseinzadeh S, Heier J. Two-dimensional MXenes for lithium-sulfur batteries. *Infomat* 2020;2:613-38. DOI
83. Yang BT, Xu MY, Gao Y, Zhu QZ, Xu B. Interfacial engineering and coupling of MXene/reduced graphene oxide/C_3N_4 aerogel with optimized d-band center as a free-standing sulfur carrier for high-performance Li-S batteries. *Small Methods* 2024;8:2301102. DOI
84. Liang X, Rangom Y, Kwok CY, Pang Q, Nazar LF. Interwoven MXene nanosheet/carbon-nanotube composites as Li-S cathode hosts. *Adv Mater* 2017;29:1603040. DOI PubMed
85. Lv LP, Guo CF, Sun W, Wang Y. Strong surface-bound sulfur in carbon nanotube bridged hierarchical Mo_2C-based MXene nanosheets for lithium-sulfur batteries. *Small* 2019;15:e1804338. DOI PubMed
86. Tang X, Gan R, Tan L, Tong C, Li C, Wei Z. 3D net-like GO-d-$Ti_3C_2T_x$ MXene aerogels with catalysis/adsorption dual effects for high-performance lithium-sulfur batteries. *ACS Appl Mater Interfaces* 2021;13:55235-42. DOI
87. Zhang S, Zhong N, Zhou X, et al. Comprehensive design of the high-sulfur-loading Li-S battery based on MXene nanosheets. *Nanomicro Lett* 2020;12:112. DOI PubMed PMC
88. Wang JL, Zhang Z, Yan XF, et al. Rational design of porous N-Ti_3C_2 MXene@CNT microspheres for high cycling stability in Li-S battery. *Nano-Micro Lett* 2020;12:4. DOI PubMed PMC
89. Song Y, Sun Z, Fan Z, et al. Rational design of porous nitrogen-doped Ti_3C_2 MXene as a multifunctional electrocatalyst for Li-S chemistry. *Nano Energy* 2020;70:104555. DOI
90. Bao W, Liu L, Wang C, Choi S, Wang D, Wang G. Facile synthesis of crumpled nitrogen-doped MXene nanosheets as a new sulfur host for lithium-sulfur batteries. *Adv Energy Mater* 2018;8:1702485. DOI
91. Yuanzheng L, Zhicheng Y, Lianghao M, Buyin L, Shufa L. A freestanding nitrogen-doped MXene/graphene cathode for high-performance Li-S batteries. *Nanoscale Adv* 2022;4:2189-95. DOI PubMed PMC
92. Zhang D, Wang S, Hu R, et al. Catalytic conversion of polysulfides on single atom zinc implanted MXene toward high-rate lithium-sulfur batteries. *Adv Funct Mater* 2020;30:2002471. DOI
93. Qin J, Wang R, Xiao P, Wang D. Engineering cooperative catalysis in Li-S batteries. *Adv Energy Mater* 2023;13:2300611. DOI
94. Tan Z, Liu S, Zhang X, et al. Few-layered V_2C MXene derived 3D V_3S_4 nanocrystal functionalized carbon flakes boosting polysulfide adsorption and catalytic conversion towards Li-S batteries. *J Mater Chem A* 2022;10:18679-89. DOI
95. Tian S, Huang J, Yang H, et al. Self-supporting multicomponent hierarchical network aerogel as sulfur anchoring-catalytic medium for highly stable lithium-sulfur battery. *Small* 2022;18:e2205163. DOI
96. Song C, Zhang W, Jin Q, Zhang Y, Wang X, Bakenov Z. In-situ constructed accordion-like Nb_2C/Nb_2O_5 heterostructure as efficient catalyzer towards high-performance lithium-sulfur batteries. *J Power Sources* 2022;520:230902. DOI
97. Zhang H, Yang L, Zhang P, et al. MXene-derived Ti_nO_{2n-1} quantum dots distributed on porous carbon nanosheets for stable and long-life Li-S batteries: enhanced polysulfde mediation via defect engineering. *Adv Mater* 2021;33:e2008447. DOI
98. Zhang M, Lu Y, Yue Z, et al. Design and synthesis of novel pomegranate-like TiN@MXene microspheres as efficient sulfur hosts for advanced lithium sulfur batteries. *RSC Adv* 2023;13:9322-32. DOI PubMed PMC
99. Wang H, Cui Z, He SA, et al. Construction of ultrathin layered MXene-TiN heterostructure enabling favorable catalytic ability for high-areal-capacity lithium-sulfur batteries. *Nano-Micro Lett* 2022;14:189. DOI PubMed PMC
100. Li T, Liang L, Chen Z, Zhu J, Shen P. Hollow Ti_3C_2T MXene@$CoSe_2$/N-doped carbon heterostructured composites for multiphase electrocatalysis process in lithium-sulfur batteries. *Chem Eng J* 2023;474:145970. DOI
101. Li J, Niu Z, Guo C, Li M, Bao W. Catalyzing the polysulfide conversion for promoting lithium sulfur battery performances: a review. *J Energy Chem* 2021;54:434-51. DOI

102. Wang L, Meng X, Wang X, Zhen M. Dual-conductive $CoSe_2$@$TiSe_2$-C heterostructures promoting overall sulfur redox kinetics under high sulfur loading and lean electrolyte. *Small* 2023;19:e2300089. DOI
103. Guo D, Ming F, Su H, et al. MXene based self-assembled cathode and antifouling separator for high-rate and dendrite-inhibited Li-S battery. *Nano Energy* 2019;61:478-85. DOI
104. Han X, Chen J, Chen M, et al. Induction of planar Li growth with designed interphases for dendrite-free Li metal anodes. *Energy Storage Mater* 2021;39:250-8. DOI
105. Yu X, Yang Y, Si L, Cai J, Lu X, Sun Z. $V_4C_3T_X$ MXene: first-principles computational and separator modification study on immobilization and catalytic conversion of polysulfide in Li-S batteries. *J Colloid Interface Sci* 2022;627:992-1002. DOI
106. Li N, Xie Y, Peng S, Xiong X, Han K. Ultra-lightweight Ti_3C_2T MXene modified separator for Li-S batteries: thickness regulation enabled polysulfide inhibition and lithium ion transportation. *J Energy Chem* 2020;42:116-25. DOI
107. Xiong D, Huang S, Fang D, et al. Porosity engineering of MXene membrane towards polysulfide inhibition and fast lithium ion transportation for lithium-sulfur batteries. *Small* 2021;17:e2007442. DOI
108. Liu P, Qu L, Tian X, et al. $Ti_3C_2T_x$/graphene oxide free-standing membranes as modified separators for lithium-sulfur batteries with enhanced rate performance. *ACS Appl Energy Mater* 2020;3:2708-18. DOI
109. Li Y, Li M, Zhu Y, et al. Polysulfide-inhibiting, thermotolerant and nonflammable separators enabled by DNA co-assembled CNT/MXene networks for stable high-safety Li-S batteries. *Compos Part B Eng* 2023;251:110465. DOI
110. Zheng M, Luo Z, Song Y, et al. Carbon-coated nitrogen, vanadium co-doped MXene interlayer for enhanced polysulfide shuttling inhibition in lithium-sulfur batteries. *J Power Sources* 2023;580:233445. DOI
111. Gu H, Yue W, Hu J, et al. Asymmetrically coordinated Cu-N_1C_2 single-atom catalyst immobilized on $Ti_3C_2T_x$ MXene as separator coating for lithium-sulfur batteries. *Adv Energy Mater* 2023;13:2204014. DOI
112. Chen D, Zhu T, Shen S, et al. In situ synthesis of VS_4/$Ti_3C_2T_x$ MXene composites as modified separators for lithium-sulfur battery. *J Colloid Interface Sci* 2023;650:480-9. DOI
113. Liang Q, Wang S, Jia X, et al. MXene derivative Ta_4C_3-Ta_2O_5 heterostructure as bi-functional barrier for Li-S batteries. *J Mater Sci Technol* 2023;151:89-98. DOI
114. Tian S, Zeng Q, Liu G, et al. Multi-dimensional composite frame as bifunctional catalytic medium for ultra-fast charging lithium-sulfur battery. *Nanomicro Lett* 2022;14:196. DOI PubMed PMC
115. Shi C, Huang J, Tang Y, et al. A hierarchical porous carbon aerogel embedded with small-sized TiO_2 nanoparticles for high-performance Li-S batteries. *Carbon* 2023;202:59-65. DOI
116. Wang Q, Liu A, Qiao S, et al. Mott-schottky MXene@WS_2 heterostructure: structural and thermodynamic insights and application in ultra stable lithium-sulfur batteries. *ChemSusChem* 2023;16:e202300507. DOI
117. Liang Q, Wang S, Lu X, et al. High-entropy MXene as bifunctional mediator toward advanced Li-S full batteries. *ACS Nano* 2024;18:2395-408. DOI
118. Wang X, Zhu B, Xu D, et al. Synergistic effects of Co_3Se_4 and $Ti_2C_3T_x$ for performance enhancement on lithium-sulfur batteries. *ACS Appl Mater Interfaces* 2023;15:26882-92. DOI
119. Li B, Zhang D, Liu Y, Yu Y, Li S, Yang S. Flexible Ti_3C_2 MXene-lithium film with lamellar structure for ultrastable metallic lithium anodes. *Nano Energy* 2017;39:654-61. DOI
120. Li W, Zhang Y, Li H, et al. Layered MXene protected lithium metal anode as an efficient polysulfide blocker for lithium-sulfur batteries. *Batteries Supercaps* 2020;3:892-9. DOI
121. Wei C, Tian M, Fan Z, et al. Concurrent realization of dendrite-free anode and high-loading cathode via 3D printed N-Ti_3C_2 MXene framework toward advanced Li-S full batteries. *Energy Storage Mater* 2021;41:141-51. DOI
122. Shi H, Zhang CJ, Lu P, Dong Y, Wen P, Wu ZS. Conducting and lithiophilic MXene/graphene framework for high-capacity, dendrite-free lithium-metal anodes. *ACS Nano* 2019;13:14308-18. DOI
123. Ren Y, Wang B, Liu H, et al. CoP nanocages intercalated MXene nanosheets as a bifunctional mediator for suppressing polysulfide shuttling and dendritic growth in lithium-sulfur batteries. *Chem Eng J* 2022;450:138046. DOI
124. Wei C, Xi B, Wang P, et al. In situ anchoring ultrafine ZnS nanodots on 2D MXene nanosheets for accelerating polysulfide redox and regulating Li plating. *Adv Mater* 2023;35:e2303780. DOI
125. Wei C, Wang Z, Wang P, et al. One-step growth of ultrathin $CoSe_2$ nanobelts on N-doped MXene nanosheets for dendrite-inhibited and kinetic-accelerated lithium-sulfur chemistry. *Sci Bull* 2024:S2095-9273(24)00199. DOI
126. Ma L, Jiang YK, Xu DR, et al. Enabling stable and low-strain lithium plating/stripping with 2D layered transition metal carbides by forming Li-zipped MXenes and a Li halide-rich solid electrolyte interphase. *Angew Chem Int Ed* 2024;63:e202318721. DOI
127. Wang C, Yang C, Du Y, Guo Z, Ye H. Spherical lithium deposition enables high Li-utilization rate, low negative/positive ratio, and high energy density in lithium metal batteries. *Adv Funct Mater* 2023;33:2303427. DOI
128. Liu Y, Meng X, Wang Z, Qiu J. Development of quasi-solid-state anode-free high-energy lithium sulfide-based batteries. *Nat Commun* 2022;13:4415. DOI PubMed PMC
129. Liu S, Chen M, Xie Y, et al. Nb_2CT_x MXene boosting PEO polymer electrolyte for all-solid-state Li-S batteries: two birds with one stone strategy to enhance Li^+ conductivity and polysulfide adsorptivity. *Rare Met* 2023;42:2562-76. DOI
130. Bao W, Wang R, Qian C, et al. Porous heteroatom-doped $Ti_3C_2T_x$ MXene microspheres enable strong adsorption of sodium polysulfides for long-life room-temperature sodium-sulfur batteries. *ACS Nano* 2021;15:16207-17. DOI
131. Wang Z, Liu Y, Guo Y, et al. Coral polyp and spine dual-inspired gradient hierarchical architecture for ultrahigh-rate and long-life

sodium storage. *Adv Funct Mater* 2024:2402178. DOI

132. Cheng Y, Huang J, Yu F, et al. Chemically bonded MXene/$SnSe_2$ composite with special structural transformation as a high-performance anode for lithium and potassium ions battery. *Chem Eng J* 2024;481:148737. DOI
133. Zheng RX, Du DY, Yan Y, Liu S, Wang XX, Shu CZ. Cation vacancy modulated interfacial electronic interactions for enhanced electrocatalysis in lithium-oxygen batteries. *Adv Funct Mater* 2024:2316440. DOI
134. Zhang H, Zhu M, Tang H, et al. A high-voltage Zn-air battery based on an asymmetric electrolyte configuration. *Energy Storage Mater* 2023;59:102791. DOI
135. Li J, Yuan X, Lin C, et al. Achieving high pseudocapacitance of 2D titanium carbide (MXene) by cation intercalation and surface modification. *Adv Energy Mater* 2017;7:1602725. DOI
136. Wang XY, Liao SY, Huang HP, et al. Enhancing the chemical stability of MXene through synergy of hydrogen bond and coordination bond in aqueous solution. *Small Methods* 2023;7:e2201694. DOI